JOURNAL OF MOLECULAR SPECTROSCOPY **110,** 215–241 (1985)

Rotational Analysis of the Red Electronic Emission Spectrum of Molybdenum Nitride (MoN)

R. C. CARLSON,[1] J. K. BATES,[2] AND T. M. DUNN

The Department of Chemistry, University of Michigan, Ann Arbor, Michigan 48109

A system of emission bands in the red region of the optical spectrum has been identified as due to the species MoN. The system was generated by the microwave (2450 MHz) excitation of a flowing mixture of $MoCl_5$ and molecular nitrogen in a stream of helium but is also observed in a DC arc in air between molybdenum electrodes. One of the *Q*-form branches has previously been assumed to be an atomic line of Mo I. The system has been assigned as the 0, 0 band of a $^4\Pi(a) \rightarrow X^4\Sigma^-(a)$ transition, with a large zero-field splitting of the ground $^4\Sigma^-$ term ($\sim$86 cm^{-1}). A preliminary search has been made to detect the presence of MoN in M-type stars.

INTRODUCTION

In contrast to the transition metal oxide emission spectra there are, so far, relatively few transition metal nitride systems either known or analyzed. The species identified in the gas phase are TiN (*1, 2*), ZrN (*3*), NbN (*4, 5*), MoN (*6, 7*), VN (*8*), TaN (*9*), and ReN (*10*), while matrix isolation studies have been carried out on TaN (*11*), ZrN (*12*), MoN (*13, 14*), and NbN (*15*). In fact, the first authenticated example of a transition metal nitride system was that of MoN, which was recognized by Howard and Conway (*6*) in 1965 from the results of an ^{15}N isotopic experiment. The systems were not, however, rotationally analyzed and, when generated by an arc between molybdenum electrodes in nitrogen, the lines are badly broadened from Doppler and multiple molybdenum isotope sources. [Natural abundance molybdenum has seven isotopes with mass numbers and abundances of 92 (15.84%), 94 (9.04%), 95 (15.72%), 96 (16.53%), 97 (9.46%), 98 (23.78%) and 100 (9.63%).]

In addition to the rarity of nitride systems, there are few examples (*16–23*) of transitions between terms with quartet spin states, particularly where there is a large zero-field splitting of a $^4\Sigma^-$ state (*24*) requiring its classification as Hund's case (a) (*25, 26*). The present example involves both of these circumstances.

Finally, it is worth noting that molybdenum appears to be unique among the transition metals in its generation of a nitride in an arc in air. The ramifications are that there may be indication of MoN in the cool (M and S type) stars, and even though this phenomenon cannot be directly connected with the role of molybdenum in nitrogen fixation by legumes it may, nonetheless, be indirectly related to it.

[1] Department of Chemistry, University of California, and Materials and Molecular Research Division, Lawrence Berkeley Laboratory, Berkeley, Calif. 94720.

[2] Chemical Technology Division, Argonne National Laboratory, Argonne, Ill. 60439.

0022-2852/85 $3.00

EXPERIMENTAL DETAILS

The spectra of all systems were obtained from the reaction of isotopically enriched (~85%) $^{94}MoCl_5$ and active nitrogen (and also $^{15}N_2$) in a microwave discharge (~100 W) using helium as the pumping gas. The spectra were photographed on 103aD, 103aF, II aD, and II aF plates and films on a 1.5-m Bausch and Lomb spectrograph for low resolution (~15 Å/mm in the first order) and in the 9th and 10th orders of a Jarrell-Ash 3.4-m Ebert spectrograph. The resolution is ~500,000 in the 10th order of the latter instrument and the reciprocal dispersion is ~3 Å/cm.

Standard wavelength calibrations used were neon, thorium (in a microwave excited discharge), and a hollow cathode Fe lamp. The standard lines were first fitted to a quadratic equation, any badly fitting lines being discarded or checked for errors. The lines were finally fitted to a fourth-order polynomial with a standard deviation of not greater than 0.001 Å, any suspect lines again being discarded. The wavelengths of the unblended spectral lines were interpolated from this polynomial, having been measured to an accuracy of ~1 μm, and were converted to vacuum wavelengths and cm^{-1}. Final errors in the line positions have been estimated as ± 0.003 cm^{-1}.

The line frequencies are listed in Tables Ia, b, c, and d in cm^{-1} (vacuum corrected).

APPEARANCE OF SYSTEM

The emission from MoN is quite intense under these experimental conditions and the discharge has a distinct reddish aureole. Under low resolution (Fig. 1) the region between 5990 and 6350 Å is dominated by molecular bands. The carrier was confirmed from the ^{15}N spectra as MoN and the bandheads closely match chose given by Howard and Conway (*6*). An exception is the intense line-like feature at 6123 Å which shows a negligible isotope shift and is identified in the MIT tables as an atomic line of Mo. As is shown below, this feature is really a complex combination of *Q*-form bandheads.

Under high resolution, the band system clearly represents one of the most spectacular examples of a high-spin multiplicity transition. Aside from some weak sequence bands there are very few interfering lines of any kind, there are no obvious perturbations, and the intensity is sufficient to allow the lines to be recorded up to $J \sim 60$.

The high-resolution photographs of the systems are given in Figs. 2a, b, c, and d. It will be immediately observed that the 6305- and 5996-Å systems are very similar in appearance, with spacings between lines at low values of J of $0B$ and $\pm 2B$. The 6245- and 6123-Å systems are also very similar, with low J spacings of $0B$, $\pm 2B$, and $\pm 4B$. (The wavelengths indicated correspond to the subband origins, ν_0.) The former pair are typical of many previously known subbands in that they consist of doubled *P*, *Q*, and *R* branches with a conventional J dependence and degradation. The latter pair are quite distinct, however, in their unusual *Q*-form, *O*, and *S*-form features in addition to the more usual *P* and *R* branches.

TABLE Ia

Line Frequencies for the $^4\Pi_{-1/2} \rightarrow {}^4\Sigma^-_{3/2}$ Transition of MoN

J	Q_{ef}	Q_{fe}	P_{ff}	P_{ee}	R_{ff}	R_{ee}
1.5	15855.822	15856.180	0.	0.	0.	0.
2.5	15855.507	15856.048	15853.460	15853.107	15859.577B	15858.914B
3.5	15855.171	15855.886	15852.328	15851.833	0.	15859.577B
4.5	15854.790	15855.687	15851.155	15850.467	15861.207B	15860.173
5.5	15854.340	15855.422	15849.861	15849.087	15861.884	15860.729
6.5	15853.815	15855.096	15848.516	15847.551	15862.531	15861.226B
7.5	15853.185	15854.695	15847.085	15845.992	15863.080B	15861.645B
8.5	15852.540	15854.251	15845.610	15844.413	15863.572	15862.034B
9.5	15851.833	15853.744	15844.063	15842.745	15863.960	15862.326B
10.5	15851.030	15853.185	15842.428	15841.031	15864.304	15862.572B
11.5	15850.147	15852.540	15840.696	15839.268	15864.583	15862.785B
12.5	15849.210	15851.833	15838.947	15837.428	0.	0.
13.5	15848.202	15851.155R	15837.088	15835.540	0.	0.
14.5	15847.113	15850.295	15835.169	15833.581	0.	0.
15.5	15845.982	15849.430	15833.169	15831.614	0.	0.
16.5	15844.755	15848.516	15831.096	15829.579	0.	0.
17.5	15843.460	15847.551	15828.789R	15827.486	15864.653	0.
18.5	15842.105	15846.525	15826.728	15825.346	15864.391	15862.785B
19.5	15840.696	15845.444	15824.430	15823.149	15864.074	15862.572B
20.5	15839.187	15844.312	15822.067	15820.918	15863.677	15862.326B
21.5	15837.617	15843.130	15819.616	15818.621	15863.207	15862.034B
22.5	15835.984	15841.891	15817.104	15816.296	15862.667	15861.645B
23.5	15834.279	15840.601	15814.511	15813.916	15862.034B	15861.226B
24.5	15832.509	15839.268	15811.863	15811.490	15861.382	15860.814
25.5	15830.675	15837.880	15809.132	15809.016	15860.626	15860.334
26.5	15828.789	15836.441	15806.342	15806.498	15859.797B	15859.797B
27.5	15826.820	15834.960	15803.463	15803.942	15858.914	15859.218
28.5	15824.787	15833.420	15800.530	15801.337	15857.939B	15858.604B
29.5	15822.692	15831.852	15797.519	15798.683	15856.919	15857.939B
30.5	15820.539	15830.223	15794.441	15796.008	15855.822	15857.195B
31.5	15818.319	15828.555	15791.326	15793.277	15854.695	15856.481
32.5	15816.045	15826.820	15788.120	15790.494	0.	15855.687B
33.5	15813.709	15825.073	15784.843	15787.695	15852.147	15854.873
34.5	15811.312	15823.268	15781.583	15784.843	15850.802	15854.006
35.5	15808.881	15821.427	15778.144	15781.945	0.	0.
36.5	15806.342	15819.528	0.	15779.007	15847.902	15852.147B
37.5	15803.792	15817.597	0.	0.	15846.389	15851.155B
38.5	15801.167	15815.624	0.	0.	15844.755B	15850.147B
39.5	15798.494	15813.611	0.	0.	15843.130B	15849.055
40.5	15795.763	15811.543	0.	0.	15841.414	15847.902
41.5	15792.962	15809.442	0.	0.	15839.660	15846.818
42.5	15790.137	15807.305	0.	0.	15837.880	15845.610
43.5	15787.267	15805.129	0.	0.	15835.984	15844.413B
44.5	15784.321	15802.912	0.	0.	15834.041	15843.130
45.5	15781.360	15800.648	0.	0.	15832.052	0.
46.5	15778.272	15798.360	0.	0.	15830.045	0.
47.5	0.	15796.008	0.	0.	15827.959	0.
48.5	0.	15793.638	0.	0.	0.	0.
49.5	0.	15791.238	0.	0.	0.	0.
50.5	0.	15788.782	0.	0.	0.	0.
51.5	0.	15786.306	0.	0.	0.	0.

B = BLENDED LINE

R = REJECTED LINE

RESULTS AND ANALYSIS

The four subbands described above have been assigned as the $^4\Pi_{-1/2}(a) \rightarrow {}^4\Sigma^-_{3/2}(a)$ (6305 Å), $^4\Pi_{1/2}(a) \rightarrow {}^4\Sigma^-_{1/2}(a)$ (6245 Å), $^4\Pi_{3/2}(a) \rightarrow {}^4\Sigma^-_{1/2}(a)$ (6123 Å), and $^4\Pi_{5/2}(a) \rightarrow {}^4\Sigma^-_{3/2}(a)$ (5996 Å) components of the (0, 0) band of a $^4\Pi(a) \rightarrow {}^4\Sigma^-(a)$ transition. This assignment was based, first, upon the general appearance of the bands, as cited above; second, by a subband by subband analysis; and, third, upon a concerted analysis of the system. The gross appearance of the system can be derived from the energy level diagram given in Fig. 1 and it reflects the case (a) selection rules $\Delta\Sigma = 0$ and $\Delta\Omega = 0, \pm 1$. It will be noted that there is a very small

TABLE Ib

Line Frequencies for the $^4\Pi_{1/2} \rightarrow {}^4\Sigma^-_{1/2}$ Transition of MoN

J	Q_{ef}	Q_{fe}	P_{ff}	P_{ee}	R_{ff}	R_{ee}
1.5	16004.792	0.	0.	0.	0.	16011.552B
2.5	16003.898	0.	0.	0.	0.	16013.692B
3.5	16003.024	16010.253	0.	0.	0.	16015.846B
4.5	16002.137B	16011.188	0.	0.	0.	16018.063
5.5	16001.269	16012.107	0.	0.	0.	16020.242
6.5	16000.406	16013.042	15992.257B	0.	0.	16022.376B
7.5	15999.559	16013.975	15990.172	0.	0.	16024.585
8.5	15998.710B	16014.912	15988.091	0.	0.	16026.755
9.5	15997.870B	16015.846	15986.022	0.	0.	16028.920
10.5	15997.046	16016.781	15983.948B	0.	0.	16031.082
11.5	15996.234	16017.714	15981.941B	0.	0.	16033.240
12.5	15995.426	16018.649	15979.892	0.	0.	16035.241R
13.5	15994.628	16019.582	15977.890	0.	0.	16037.534
14.5	15993.844	16020.514	15975.881B	0.	0.	16039.678
15.5	15993.070	16021.445	15973.887B	0.	0.	16041.809
16.5	15992.305	16022.376	15971.938	0.	16006.423	16043.925
17.5	15991.549	16023.293	15969.985	0.	16006.515	16046.028B
18.5	15990.813	16024.212	15968.054	0.	16006.628	16048.235R
19.5	15990.079	16025.122	15966.115B	0.	16006.742	16050.238
20.5	15989.352	16026.031	15964.236B	0.	16006.872	16052.317
21.5	15988.648	16026.928	15962.347	0.	16007.015	16054.389
22.5	15987.944	16027.821	15960.443B	0.	16007.177	16056.448
23.5	15987.252	16028.709	15958.624	0.	16007.353	16058.491
24.5	15986.567	16029.586	0.	0.	0.	16060.525
25.5	15985.896	16030.455	15954.937	0.	0.	16062.546
26.5	15985.228	16031.311	15953.127	0.	0.	16064.542
27.5	15984.565	16032.159	15951.304	0.	16008.170	16066.532
28.5	15983.913B	16032.997	0.	0.	0.	16068.504
29.5	15983.261	16033.819	0.	0.	0.	16070.458
30.5	15982.617	16034.635	0.	0.	0.	16072.399
31.5	15981.974B	16035.421B	0.	0.	0.	16074.320
32.5	15981.346	16036.218	0.	0.	0.	16076.222
33.5	15980.703	16036.990	0.	0.	16009.658	16078.112
34.5	15980.071	16037.749	0.	0.	16009.927	16079.971
35.5	15979.427	16038.486	0.	0.	16010.215	16081.817
36.5	15978.804	16039.213	0.	16008.445	16010.471	16083.643
37.5	15978.160	16039.926	0.	16008.243	16010.749	16085.442
38.5	15977.522	16040.617	0.	16008.028	16011.017	16087.226
39.5	15976.871	16041.288	0.	16007.784	16011.283	16088.995
40.5	0.	16041.942	0.	0.	16011.552B	16090.730
41.5	15975.554	16042.584	0.	16007.256	16011.820	16092.451
42.5	15974.903	16043.201	0.	16006.933	0.	16094.145
43.5	15974.228	16043.799	0.	16006.626	0.	16095.814
44.5	0.	16044.379	0.	0.	0.	16097.465
45.5	0.	16044.937	0.	16005.930	0.	16099.090
46.5	0.	16045.476	0.	16005.538	0.	16100.687
47.5	0.	16045.995B	0.	16005.127	0.	16102.261
48.5	0.	16046.482	0.	16004.685	0.	16103.814
49.5	0.	16046.956	0.	16004.225	0.	16105.336
50.5	0.	16047.405	0.	16003.738	0.	16106.829
51.5	0.	16047.833	0.	16003.233	0.	16108.301
52.5	0.	16048.142R	0.	16002.699	0.	16109.752
53.5	0.	16048.613	0.	16002.137B	0.	16111.169
54.5	0.	16048.976	0.	16001.546	0.	16112.560
55.5	0.	16049.299	0.	16000.941	0.	16113.927
56.5	0.	16049.611	0.	0.	0.	16115.259
57.5	0.	16049.888	0.	0.	0.	16116.578
58.5	0.	16050.138	0.	0.	0.	16117.826
59.5	0.	16050.371	0.	0.	0.	16119.097
60.5	0.	16050.583	0.	0.	0.	16120.325

interval for the $^4\Pi_{1/2} \rightarrow {}^4\Pi_{-1/2}$ spacing ($\sim$65 cm^{-1}) but that the spacings for the other $^4\Pi$ components are as would be expected for a second-row transition element with a one-electron spin–orbit coupling constant $\sim$300 cm^{-1}. Perhaps the most surprising feature is the very large zero-field splitting of the $^4\Sigma^-$ state, $\sim$86 cm^{-1}, thereby clearly classifying it as an example of Hund's case (a) coupling. The very

TABLE Ic

Line Frequencies for the $^4\Pi_{3/2} \rightarrow {}^4\Sigma^-_{1/2}$ Transition of MoN

J	Q_{ef}	Q_{fe}	P_{ff}	P_{ee}	R_{ff}	R_{ee}
.5						16327.599
1.5	0.	16327.107	0.	0.	0.	16329.621
2.5	0.	16328.105	0.	0.	0.	16331.641
3.5	16320.960	16329.110	0.	0.	0.	16333.657
4.5	16319.905	16330.105	0.	0.	0.	16335.660
5.5	16318.862	16331.091	16313.309	0.	0.	0.
6.5	16317.826	16332.069	16311.268	0.	0.	16339.641
7.5	16316.787	16333.039	16309.214	0.	0.	16341.624
8.5	16315.747	16333.993	16307.160	0.	0.	16343.599
9.5	16314.707B	16334.941	16305.106	0.	0.	16345.552
10.5	16313.680	16335.878	16303.056	0.	0.	0.
11.5	16312.644	16336.804	16301.027	0.	0.	16349.436
12.5	16311.617	16337.718	16298.979	0.	0.	16351.355
13.5	16310.592	16338.613	16296.949	16324.976	0.	0.
14.5	16309.572	16339.502	16294.923B	16324.862	0.	16355.164
15.5	16308.552	16340.379	0.	16324.729	0.	0.
16.5	16307.530	16341.235	16290.872	16324.564	0.	16358.905
17.5	16306.534	16342.076	16288.830	16324.418	0.	16360.768
18.5	16305.533	16342.912	16286.835	16324.242	0.	16362.611
19.5	16304.530	16343.723	0.	16324.046	0.	16364.428
20.5	16303.542	16344.521	16282.820	16323.922	0.	16366.237
21.5	16302.557	16345.204R	16280.830	16323.610	0.	16368.022
22.5	16301.579	16346.066	16278.839	16323.371	0.	16369.804
23.5	16300.601	16346.820	16276.855	16323.119	0.	16371.559
24.5	16299.629	16347.528B	16274.876	16322.845	0.	16373.299
25.5	16298.663	16348.262	16272.898	16322.553	0.	16375.023
26.5	16297.698	16348.962	16270.929	16322.242	0.	16376.729
27.5	16296.743	16349.638	16268.955	16321.927	0.	16378.415
28.5	16295.786	16350.252B	16266.999	16321.516B	0.	16380.085
29.5	16294.831B	16350.939	16265.021	16321.228	0.	16381.737
30.5	16293.891	16351.562	16263.087	16320.843	0.	16383.369
31.5	16292.921	16352.170	16261.119	16320.450	0.	16384.980
32.5	16291.993	16352.749	16259.163	16320.032	0.	16386.575
33.5	16291.045	16353.298	16257.210	16319.600	0.	16388.145
34.5	16290.096	16353.864	16255.255	16319.139	0.	16389.701
35.5	16289.147	16354.388	16253.292	16318.668	0.	16391.236
36.5	16288.194	16354.889	16251.348	16318.175	0.	16392.749
37.5	16287.246	16355.372	16249.380	16317.662	0.	16394.238
38.5	16286.289	16355.835	16247.416	16317.134	0.	16395.706
39.5	16285.336	16356.285	16245.447	16316.580	0.	16397.151
40.5	16284.364	16356.703	16243.473	16316.004	0.	16398.587
41.5	16283.402	0.	16241.490	16315.412	0.	16399.991
42.5	16282.422	16357.481	16239.518	16314.790B	0.	16401.373
43.5	0.	16357.840	16237.531	16314.166	0.	16402.744
44.5	16280.455	16358.178	16235.538	16313.510	0.	16404.083
45.5	16279.456	16358.489	16233.532	16312.831	0.	16405.401
46.5	16278.443	16358.783	16231.522	16312.142	0.	16406.701
47.5	16277.434	16359.054	16229.498	16311.416B	0.	16407.973
48.5	16276.415	16359.306	16227.475	16310.678B	0.	16409.230
49.5	16275.373	16359.531	16225.424	16309.916	0.	16410.457
50.5	16274.325	16359.734	16223.384	16309.134	0.	16411.663
51.5	16273.281	16359.912	16221.321	16308.337	0.	16412.847
52.5	0.	16360.074	16219.238	0.	0.	16414.004
53.5	16271.117	16360.208	16217.164	16306.651	0.	16415.138
54.5	16270.020	0.	16215.068	16305.782	0.	16416.253
55.5	16268.922	0.	16212.959	16304.895	0.	16417.348
56.5	16267.786	0.	16210.812	16303.980	0.	16418.412
57.5	16266.651	0.	16208.686	0.	0.	16419.451
58.5	16265.490	0.	0.	16302.081	0.	16420.473
59.5	16264.325	0.	16204.366	16301.085B	0.	16421.473
60.5	0.	0.	16202.175	16300.098	0.	16422.448

unusual appearance of the *Q*-form (line-like) features in the 6123- and 6245-Å subbands is the result of the combination of a large Ω-type splitting of the $^4\Sigma^-_{1/2}$ state upon which both terminate and the Λ-doubling of the $^4\Pi$ substates from which the transitions arise.

The analysis of the spectrum has been performed in three successive stages: the subband by subband analysis ($^4\Pi_\Omega \rightarrow {}^4\Sigma^-_\Omega$), the intermediate analysis [$^4\Pi_\Omega \rightarrow {}^4\Sigma^-(a)$],

TABLE Id

Line Frequencies for the $^4\Pi_{5/2} \rightarrow {}^4\Sigma^-_{3/2}$ Transition of MoN

J	Q_{ef}	Q_{fe}	P_{ff}	P_{ee}	R_{ff}	R_{ee}
1.5	0.	0.	0.	0.	16675.446	0.
2.5	16672.830B	16672.830B	0.	0.	16676.364	0.
3.5	16672.684B	16672.684B	0.	0.	16677.233	0.
4.5	16672.494B	16672.494B	0.	0.	16678.067	0.
5.5	16672.274B	16672.274B	0.	0.	16678.852	0.
6.5	16671.987	16672.063	16665.409	16665.485	16679.574	16679.655
7.5	16671.658	16671.771	0.	0.	16680.259	16680.365
8.5	16671.288	16671.450	0.	16662.839	16680.913	16681.052
9.5	16670.870	16671.095	16661.256	16661.480	16681.503	16681.716
10.5	16670.411	16670.712	16659.798	16660.096	16682.051	16682.336
11.5	16669.897	16670.282	16658.282	16658.649	16682.562	16682.925
12.5	16669.340	16669.828	16656.713	16657.189	16682.999	16683.478
13.5	16668.742	16669.340	0.	16655.685	16683.412	16684.023
14.5	16668.088	16668.814	16653.417	16654.157	16683.769	0.
15.5	16667.380	16668.263	16651.700	16652.584	0.	16684.953
16.5	16666.621	16667.679	16649.930	16650.993	0.	16685.367
17.5	16665.817	16667.067	16648.122	16649.348	0.	16685.754
18.5	16664.956	16666.419	0.	16647.723	0.	16686.130
19.5	16664.056	16665.742	16644.326	16646.026	0.	16686.474
20.5	16663.104	16665.033	16642.386	16644.326	0.	16686.777
21.5	16662.097	16664.300	16640.357	16642.544	0.	16687.049
22.5	16661.063	16663.535	16638.302	16640.786	0.	16687.299
23.5	16659.941	16662.742	16636.180	16638.988	16684.698	16687.516
24.5	16658.786	16661.924	16634.020	16637.156	16684.550	16687.703
25.5	16657.578	16661.063	16631.807	16635.310	16684.342	16687.855
26.5	16656.328	16660.193	16629.492R	16633.419	0.	0.
27.5	16655.030	16659.289	16627.240	16631.503	0.	0.
28.5	16653.673	16658.358	16624.885	16629.492	0.	0.
29.5	16652.273	16657.398	16622.469	16627.598	0.	0.
30.5	16650.829	16656.411	16620.023	16625.598	0.	0.
31.5	16649.348	16655.391	16617.519	16623.584	0.	0.
32.5	16647.802	16654.356	16614.968	16621.540	0.	0.
33.5	16646.229	16653.288	16612.390	16619.464	16681.052	0.
34.5	16644.595	16652.196	16609.757	16617.356	16680.431	0.
35.5	16642.919	16651.075	16607.087	16615.240	16679.770	0.
36.5	16641.206	16649.930	16604.372	16613.074	16679.051	16687.776
37.5	16639.449	16648.760	16601.592	16610.907	16678.297R	16687.616
38.5	16637.648	16647.569	16598.804	16608.713	16677.507	16687.423
39.5	16635.805	16646.343	16595.960	16606.502	16676.668	16687.193
40.5	16633.927	16645.099	16593.071	16604.245	16675.785	16686.961
41.5	16632.007	16643.829	16590.155	16601.970	16674.874	16686.694
42.5	16630.053	16642.544	16587.188	16599.672	16673.913	16686.395
43.5	16628.059	16641.206	16584.196	16597.358	16672.928	16686.069
44.5	16626.018	16639.867	16581.157	16595.011	16671.887	16685.754
45.5	16623.953	16638.504	0.	16592.630	16670.822	16685.367
46.5	16621.855	16637.110	16574.995	16590.247	16669.704	16684.953
47.5	16619.686	16635.698	16571.854	16587.858	16668.568	0.
48.5	16617.519	16634.232	16568.669	16585.393	0.	0.
49.5	16615.317	16632.784	16565.455	16582.934	16666.166	16683.642
50.5	16613.074	16631.304	16562.219	16580.451	0.	0.
51.5	16610.796	16629.783	16558.947	0.	16663.633	16682.641
52.5	16608.483	16628.251	16555.626	16575.405	16662.316	0.
53.5	16606.145	16626.680	16552.310	16572.859	0.	0.
54.5	16603.769	16625.113	16548.935	16570.291	16659.606	0.
55.5	16601.364	0.	16545.536	16567.672	0.	0.
56.5	16598.928	0.	0.	16565.064	0.	0.
57.5	16596.457	16620.231	16538.641	16562.427	0.	16679.051
58.5	16593.952	16618.566	0.	16559.750	0.	16678.297
59.5	16591.450	16616.865	16531.647	16557.068	16652.273	16677.660
60.5	16588.906	16615.143	16528.106	16554.354	0.	16676.932
61.5	16586.322R	16613.391	0.	0.	16649.099R	16676.179

and the complete analysis [$^4\Pi(a) \rightarrow {}^4\Sigma^-(a)$]. In the first of these stages, the molecular constants for each individual $^4\Pi_\Omega$ and $^4\Sigma^-_\Omega$ substate are calculated from combination relations. This is necessary to confirm the relationship between the various subbands, and also accentuates the differences between individual subband constants. Additionally, the recognition of individual subbands by other workers necessitates listing their separate constants.

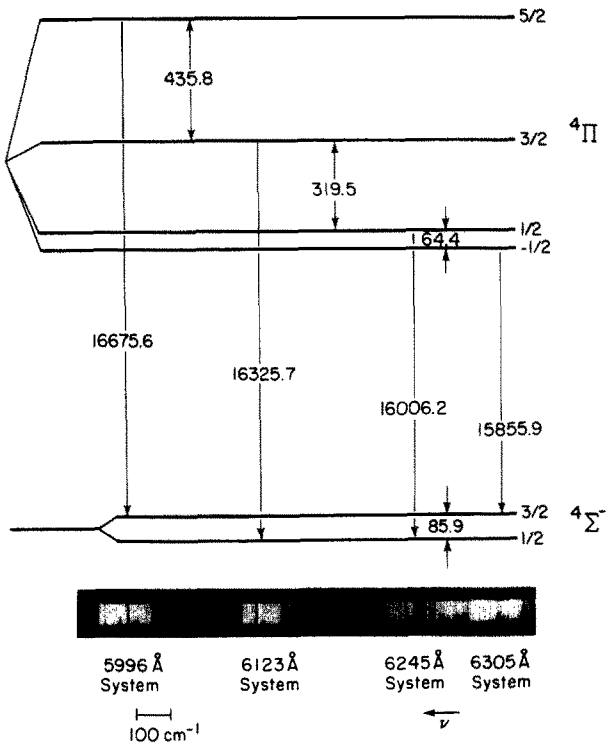

FIG. 1. Low-resolution spectrum and energy level diagram for the $^4\Pi(a) \rightarrow {}^4\Sigma^-(a)$ transition in MoN.

In the second stage, the molecular constants for the $^4\Sigma^-(a)$ state are calculated from combination relations and, using these values, greatly improved values for the $^4\Pi_\Omega$ substate constants are then obtained from direct fits to the frequencies of the corresponding subbands. In the final stage, the 1003 line frequencies comprising all four subband systems are fitted to the corresponding differences between the eigenvalues of the $^4\Pi(a)$ and $^4\Sigma^-(a)$ Hamiltonian matrices in order to calculate constants for the $^4\Pi(a)$ state.

$^4\Pi$ *State*

The Hamiltonian for each vibrational level of a $^4\Pi$ state may be written as (*18*)

$$H = {}^eT_v + H_{so} + H_{rot} + H_{ss} + H_{sr} + H_A, \tag{1}$$

where

$${}^eT_v = \text{the electronic and vibrational energy}$$

$$H_{so} = A_v L_z S_z + 1/2 A_{D_v}(\tilde{R}^2 L_z S_z + L_z S_z \tilde{R}^2).$$

The first term in H_{so} is the spin–orbit interaction, and the second term is its centrifugal distortion correction.

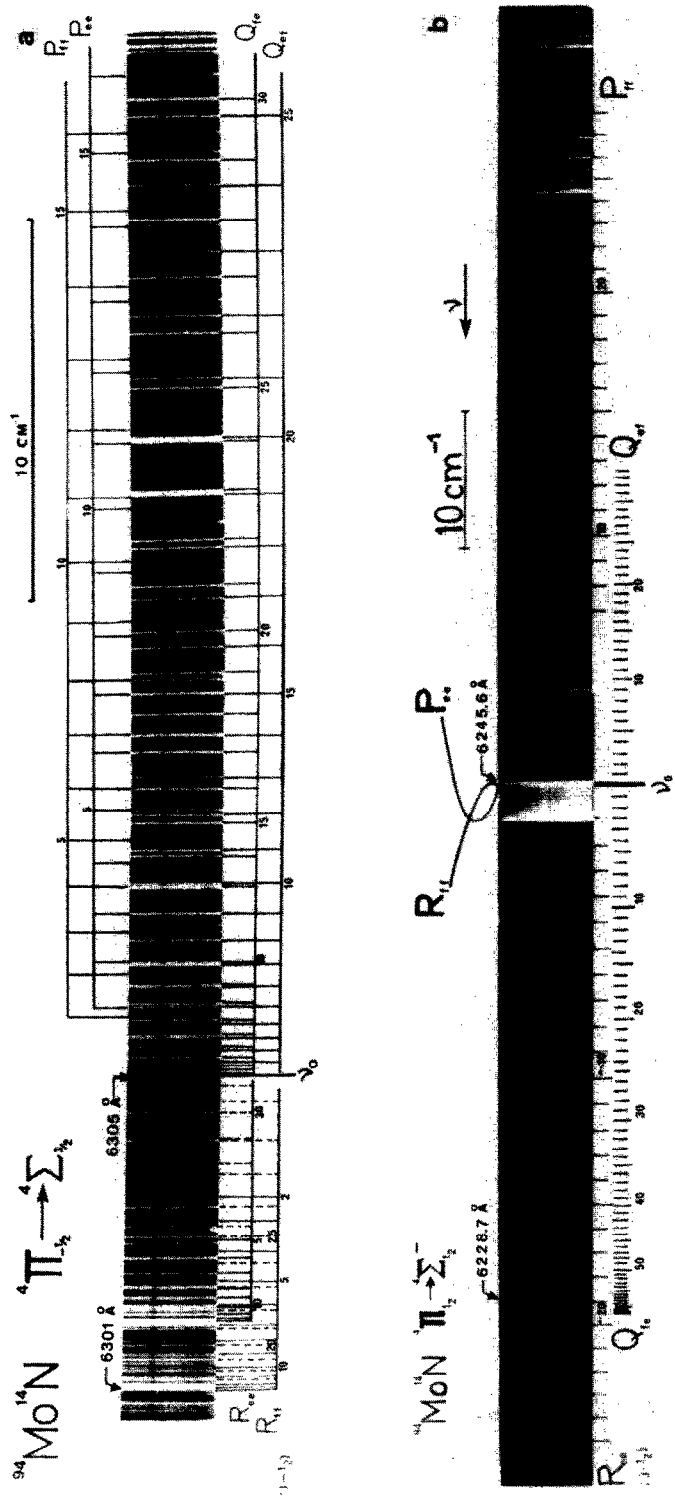

FIG. 2. (a) High-resolution spectrum of the $^4\Pi_{-1/2} \rightarrow {}^4\Sigma_{3/2}^-$ transition in the red system of ^{94}MoN. (b) High-resolution spectrum of the $^4\Pi_{1/2} \rightarrow {}^4\Sigma_{1/2}^-$ transition in the red system of ^{94}MoN. (c) High-resolution spectrum of the $^4\Pi_{3/2} \rightarrow {}^4\Sigma_{1/2}^-$ transition in the red system of ^{94}MoN. (d) High-resolution spectrum of the $^4\Pi_{5/2} \rightarrow {}^4\Sigma_{3/2}^-$ transition in the red system of ^{94}MoN.

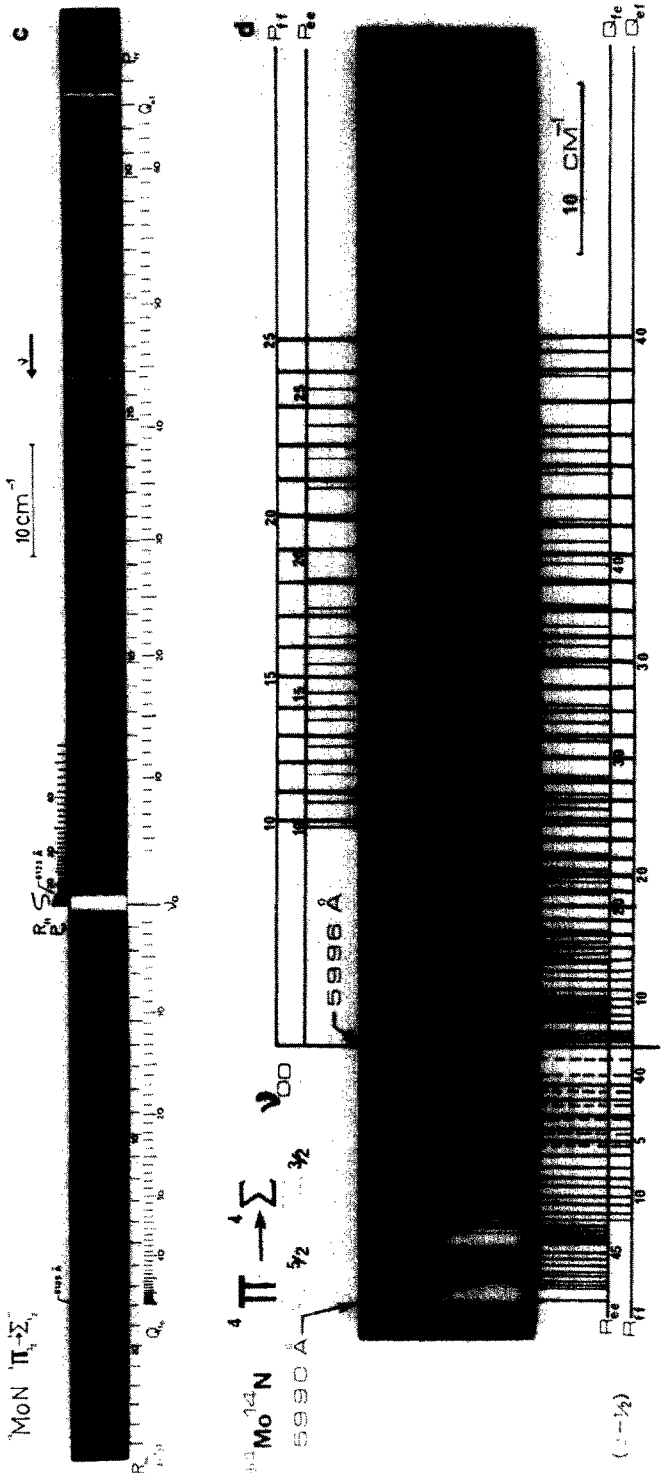

FIG. 2—*Continued.*

$$H_{\text{rot}} = B_v(\tilde{J} - \tilde{L} - \tilde{S})^2 - D_v(\tilde{J} - \tilde{L} - \tilde{S})^4$$

B_v is the rotational constant, and D_v is its first centrifugal distortion correction.

$$H_{\text{ss}} = \epsilon_v(3\tilde{S}_z^2 - \tilde{S}^2) + 1/2\alpha_v(S_+S_+ + S_-S_-)\delta_{0,\Delta\Omega}$$

The first and second terms of H_{ss} are the parts of the spin–spin interaction which are diagonal and nondiagonal, respectively, in Λ.

$$H_{\text{sr}} = \gamma_v(\tilde{J} - \tilde{S})\cdot\tilde{S}$$

is the spin–rotation interaction diagonal in Λ.

$$H_\Lambda = 1/2q_v(J_+ + J_-)^2 + (1/2q_v + 1/2p_v + o_v)(S_+ + S_-)^2 - (1/2q_v + 1/4p_v)[(J_+ + J_-)(S_+ + S_-) + (S_+ + S_-)(J_+ + J_-)]$$

is the lambda-doubling interaction. The lambda-doubling constants p_v, q_v, and o_v are defined by Zare *et al.* (*20*). They show that o_v cannot be obtained experimentally but, instead, is approximated by

$$o_v = 1/8(A_v/B_v)p_v$$

The set of case (a) basis functions of definite parity $|\Omega\pm\rangle$ are, for a $^4\Pi$ state,

$$\begin{aligned}
|-1/2\pm\rangle &= 2^{-1/2}[|1, -3/2\rangle \pm |-1, 3/2\rangle] \\
|1/2\pm\rangle &= 2^{-1/2}[|1, -1/2\rangle \pm |-1, 1/2\rangle] \\
|3/2\pm\rangle &= 2^{-1/2}[|1, 1/2\rangle \pm |-1, -1/2\rangle] \\
|5/2\pm\rangle &= 2^{-1/2}[|1, 3/2\rangle \pm |-1, -3/2\rangle]
\end{aligned} \tag{2}$$

The plus and minus signs refer to the e and f rotational levels, respectively, where the e, f notation is according to Kopp and Hougen, (*22*) i.e., that rotational levels with parity $+(-1)^{J-1/2}$ are designated "e" and those with parity $-(-1)^{J-1/2}$ are designated "f." With (2) as the basis set, the $^4\Pi$ Hamiltonian reduces to two 4×4 symmetric matrices, one for the e and one for the f levels.

In the MoN molecule, perturbations from one or more unidentified electronic states cause the energy differences between the $^4\Pi$ substates to differ markedly from each other, as can be seen from Fig. 1. The states causing these dramatic shifts in the substate energies have not been identified and, therefore, cannot be characterized. Accordingly, the diagonal matrix elements in (*18*) were modified in an empirical manner in order to take into account the effects of these perturbations. This was accomplished by replacing ${}^eT_v$ in each diagonal element by $T_\Omega(\Omega = -1/2, 1/2, 3/2, 5/2)$, where T_Ω is a constant term which is different for each substate. The four T_Ω's become adjustable parameters in the nonlinear least-squares fit of the eigenvalue differences to the 1003 line frequencies, as described below. The modified elements of the $^4\Pi$ matrix are given in Table II.

$^4\Sigma^-$ *State*

The Hamiltonian for each vibrational level of a $^4\Sigma^-$ state can be written as (*16, 17*)

TABLE II

Modified Matrix Elements of the $^4\Pi$ Hamiltonian in a Parity Case (a) Basis Set

$$\langle 5/2\pm|H|5/2\pm\rangle = T_{5/2} + 3/2A_v + 3\varepsilon_v + 1/2q_v + (B_v + 3/2A_{Dv} + 1/2q_v)(z^2-5) - D_v(z^4-7z^2+13)$$

$$\langle 5/2\pm|H|3/2\pm\rangle = (3)^{1/2}(z^2-4)^{1/2}[B_v + A_{Dv} - 1/2\gamma_v + 1/2q_v + 1/4p_v - 2D_v(z^2-2)]$$

$$\langle 5/2\pm|H|1/2\pm\rangle = -(12)^{1/2}D_v(z^2-1)^{1/2}\ (z^2-4)^{1/2}$$

$$\langle 5/2\pm|H|-1/2\pm\rangle = \pm\ 1/2q_v(z^2-1)^{1/2}\ (z^2-4)^{1/2}$$

$$\langle 3/2\pm|H|3/2\pm\rangle = T_{3/2} + 1/2A_v - 3\varepsilon_v + 1/2q_v + 3/2p_v + 3o_v + (B_v + 1/2A_{Dv} + 1/2q_v)(z^2+1) - D_v(z^4+9z^2-15) - 3\gamma_v$$

$$\langle 3/2\pm|H|1/2\pm\rangle = 2(z^2-1)^{1/2}[B_v - 1/2\gamma_v + 1/2q_v + 1/4p_v \pm 1/4q_v z - 2D_v(z^2+2)]$$

$$\langle 3/2\pm|H|-1/2\pm\rangle = (3)^{1/2}(z^2-1)^{1/2}[\pm(q_v + 1/2p_v) - 2D_v z]$$

$$\langle 1/2\pm|H|1/2\pm\rangle = T_{1/2} - 1/2A_v - 3\varepsilon_v - 4\gamma_v + 1/2q_v + 2p_v + 4o_v + (B_v - 1/2A_{Dv} + 1/2q_v)(z^2+3) \pm (2q_v + p_v)z - D_v(z^4+13z^2+5)$$

$$\langle 1/2\pm|H|-1/2\pm\rangle = (3)^{1/2}[\pm(\alpha_v + q_v + p_v + 2o_v) + (B_v - 1/2\gamma_v - A_{Dv} + 1/2q_v + 1/4p_v)z - 2D_v z(z^2+2)]$$

$$\langle -1/2\pm|H|-1/2\pm\rangle = T_{-1/2} - 3/2A_v + 3\varepsilon_v - 3\gamma_v + 1/2q_v + 3/2p_v + 3o_v + (B_v - 3/2A_{Dv} + 1/2q_v)(z^2+1) - D_v(z^4+5z^2+1)$$

$z = J + 1/2$

$$H = {}^eT_v + H_{\text{rot}} + H_{\text{ss}} + H_{\text{sr}} + H_{\text{so}} \tag{3}$$

${}^eT_v$, H_{rot}, and H_{sr} have the same meaning as for a $^4\Pi$ state.

$$H_{\text{ss}} = 2/3\lambda(3S_z^2 - \tilde{S}^2)$$

is that part of the spin–spin interaction which is diagonal in Λ, and

$$H_{\text{so}} = \sum_i a_i \vec{l}_i \cdot \vec{s}_i$$

is the second-order spin–orbit interaction and is not diagonal in Λ or S.

The parity case (a) basis functions $|\Omega\pm\rangle$ for a $^4\Sigma^-$ state, are

$$|1/2\pm\rangle = 2^{-1/2}[|0, 1/2\rangle \pm |0, -1/2\rangle]$$

$$|3/2\pm\rangle = 2^{-1/2}[|0, 3/2\rangle \pm |0, -3/2\rangle] \tag{4}$$

Using this basis set the 4×4 $^4\Sigma^-$ Hamiltonian matrix reduces to two 2×2 matrices, one for the e and one for the f rotational levels. The matrix elements are given in Table III. The 2×2 matrices are easily diagonalized analytically to obtain their eigenvalues, which are, respectively, the e and f rotational levels of the $^4\Sigma^-_{1/2}$ and $^4\Sigma^-_{3/2}$ substates.

The spin–spin and spin–rotation interactions have the same quantum number dependence as the second-order spin–orbit interaction (*16, 17*). In addition, the spin–spin and spin–rotation parameters are considerably smaller than the contributions to the eigenvalues from the off-diagonal elements of the spin–orbit interaction. Thus, the parameter λ can be considered as an "effective" spin-splitting parameter; most of the contributions to it are from the off-diagonal spin–orbit effects. λ is defined so that ${}^eT_0(^4\Sigma^-_{3/2}) - {}^eT_0(^4\Sigma^-_{1/2}) = 4\lambda$.

Preliminary Analysis (Subband by Subband): $^4\Pi_\Omega \rightarrow {}^4\Sigma^-_\Omega$

On the assumption of the transition as $^4\Pi(a) \rightarrow {}^4\Sigma^-(a)$ and utilizing the usual selection rules, the energy level diagram is as given in Fig. 3.

TABLE III

Matrix Elements of the $^4\Sigma$ Hamiltonian in a Parity Case (a) Basis Set

$$\langle 1/2^{\pm}|H|1/2^{\pm}\rangle = T_0 - 2\lambda + (B-4\lambda_J)(Z+4)$$

$$\mp 2(B-4\lambda_J-1/2\gamma_2)(J+1/2)$$

$$-D[(Z+4)^2 + 3Z + 4(J+1/2)^2$$

$$\mp 4(Z+4)(J+1/2)]$$

$$\langle 3/2^{\pm}|H|3/2^{\pm}\rangle = T_0 + 2\lambda + (B+4\lambda_J)Z - D(Z^2+3Z)$$

$$\langle 1/2^{\pm}|H|3/2^{\pm}\rangle = -(3Z)^{1/2}[B-1/2\gamma_1-D\{2(Z+4)\mp 2(J+1/2)\}]$$

$$Z = (J-1/2)(J+3/2)$$

As is shown by Kopp and Hougen (*25*), the rotational levels for a $^{2S+1}\Sigma_{1/2}(a)$ state are approximately expressible as

$$F_{1/2,\substack{e\\f}}(J) = B_{1/2}J(J+1) \mp 1/2p_{1/2}(J+1/2), \tag{5}$$

where the Ω-doubling constant $p = \mp(-1)^{S+1/2}(2S+1)B_{1/2}$ for $\Lambda = 0^{\pm}$, and $p = 0$ for $\Lambda \neq 0$. (For a $^4\Sigma^-_{1/2}$ state, $p = +4B_{1/2}$.) Similarly, the approximate formula for the $^4\Pi(a)$ state may be written (*27*) (for $A > 0$)

$$F_{\Omega,\substack{e\\f}}(J) = B_\Omega J(J+1) \pm 1/2p_\Omega(J+1/2) \mp \cdots, \tag{6}$$

where p_Ω is the lambda-doubling constant. When the line frequencies of the six branches Q_{ef}, Q_{fe}, ..., R_{ee} are calculated using Eqs. (5) and (6), assuming that

(i) $B'_\Omega \sim B''_\Omega \sim B$

(ii) $p''_\Omega = (p''_{1/2}) \sim 4B''_\Omega \sim 4B$

(iii) $p''_\Omega \gg p'_\Omega$

spacings of 0B, $\pm 2B$, and $\pm 4B$ are obtained for these branches, which terminate upon the $^4\Sigma^-_{1/2}$ substate. It may easily be verified that branches terminating upon the $^4\Sigma^-_{3/2}$ substate have only $0B$ and $\pm 2B$ spacings with the same assumptions.

(a) The $^4\Sigma^-$ state. One can generalize the Kopp and Hougen equation (5) as follows:

$$F''_{\Omega,\substack{e\\f}}(J) = B''_\Omega J(J+1) - D''_\Omega J^2(J+1)^2 \mp 1/2p''_\Omega(J+1/2)$$

$$\pm 1/2p''_{J,\Omega}(J+1/2)^3 \mp 1/2p''_{JJ,\Omega}(J+1/2)^5 \pm \cdots, \tag{7}$$

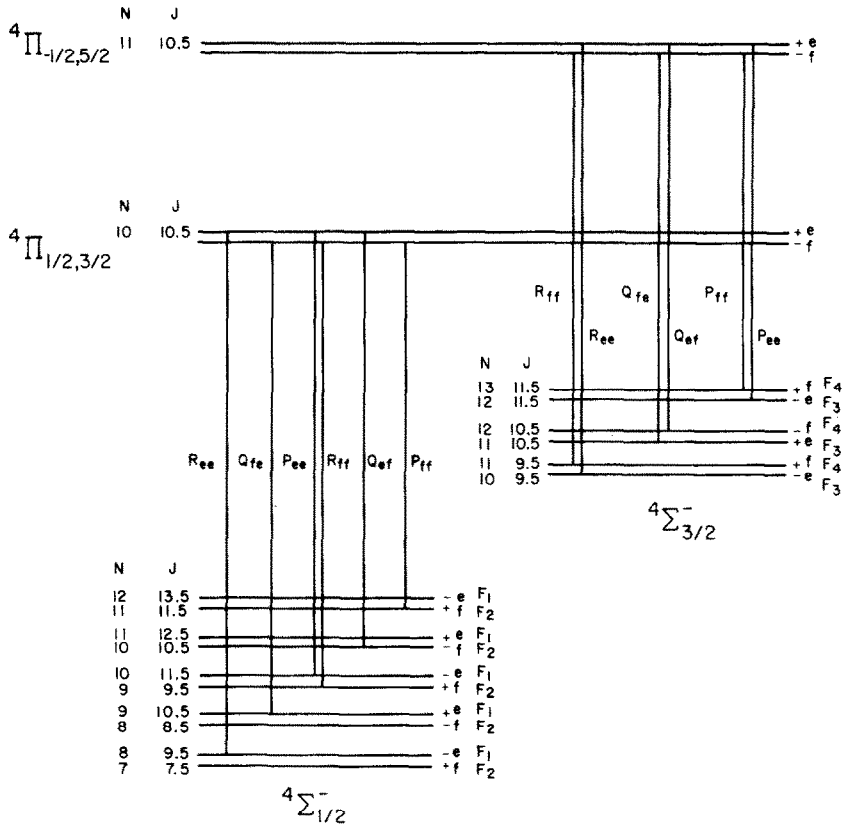

FIG. 3. Rotational energy level diagram for a $^4\Pi(a) \rightarrow {}^4\Sigma^-(a)$ transition. Note that the upper set of levels refers to the two components $^4\Pi_{-1/2}$ and $^4\Pi_{5/2}$ while the lower is for $^4\Pi_{1/2}$ and $^4\Pi_{3/2}$.

where $p''_{J,\Omega}$ and $p''_{JJ,\Omega}$ are higher-order Ω-doubling constants. Reference to Fig. 3 enables the combination relations (*A*2) given in the Appendix to be fitted to polynomials of the second degree in $(J + 1)^2$, yielding B''_Ω and D''_Ω as given in Table V.

(b) The $^4\Pi$ *state.* Generalizing Eq. (6) yields (for $A > 0$)

$$F'_{\substack{\Omega,e \\ f}}(J) = B'_\Omega J(J+1) - D'_\Omega J^2(J+1)^2 \pm 1/2p'_\Omega(J+1/2)$$

$$\mp 1/2p'_{J,\Omega}(J+1/2)^3 \pm 1/2p'_{JJ,\Omega}(J+1/2)^5 \mp \cdots. \quad (8)$$

As in the case of the $^4\Sigma^-$ state, fits to suitable combination relations (A4) enable the analogous $^4\Pi_\Omega$ constants to be calculated. These are given in Table IV.

Examination of Table IV shows that the B'_Ω and D'_Ω values have no obvious pattern, the D' value for $\Omega = -1/2$ being, apparently, negative. Nor can the constants be fitted to a relationship of the form known for $^2\Pi$ and $^3\Pi$ states, i.e.,

$$B_\Omega = B_v\left(1 + \frac{2\Sigma B_v}{A\Lambda} + \cdots\right) \quad (9)$$

TABLE IV

Molecular Constants for the $^4\Pi_\Omega$ Substates Obtained from Least-Squares Fits to Combination Differences of Each Subband (cm^{-1})

Substate	B	D	p	p_J	p_{JJ}
$^4\Pi_{-1/2}$	0.49400	-2.29×10^{-7}	-0.17356	-5.20×10^{-5}	-9.15×10^{-9}
$^4\Pi_{1/2}$	0.51041	1.13×10^{-6}	0.22549	4.86×10^{-5}	6.76×10^{-9}
$^4\Pi_{3/2}$	0.50532	5.46×10^{-7}	1.9×10^{-5}	-7.8×10^{-7}	-5.2×10^{-11}
$^4\Pi_{5/2}$	0.50593	4.14×10^{-7}	-2.3×10^{-4}	-7.7×10^{-7}	-3.6×10^{-10}

where the symbols have their usual significance. Thus, Table IV shows that a value of B_v cannot be obtained from the B_Ω's and their appropriate Σ values, unless the higher terms in the expression, which are usually small, are unexpectedly large.

The constants in Table IV and V, along with the subband origins, ν_0, were then used to calculate the frequencies of the six branches of each of the $^4\Pi_{5/2} \rightarrow {}^4\Sigma^-_{3/2}$, $^4\Pi_{3/2} \rightarrow {}^4\Sigma^-_{1/2}$, $^4\Pi_{1/2} \rightarrow {}^4\Sigma^-_{1/2}$, and $^4\Pi_{-1/2} \rightarrow {}^4\Sigma^-_{3/2}$ transitions. The origins, ν_0, were obtained from fits of $Q_{ef}(J) + Q_{fe}(J)$ to polynomials of third degree in J. In all four subbands the calculated frequences agree with their measured counterparts to within $\sim$0.2 cm^{-1} for small values of J. However, as J increases to 60.5 the differences become as large as 1 cm^{-1} for the 6305-Å subband, 8 cm^{-1} for the 6245- and 5996-Å subbands, and 12 cm^{-1} for the 6123-Å subband!

TABLE V

$^4\Sigma^-$ Molecular Constants Obtained from Least-Squares Fits to Combination Differences (cm^{-1})

	$^4\Sigma^-_{1/2}$		$^4\Sigma^-_{3/2}$		$^4\Sigma^-$	
	$^4\Pi_{1/2} + {}^4\Sigma^-_{1/2}$	$^4\Pi_{3/2} + {}^4\Sigma^-_{1/2}$	$^4\Pi_{-1/2} + {}^4\Sigma^-_{3/2}$	$^4\Pi_{5/2} + {}^4\Sigma^-_{3/2}$	$^4\Pi(a) + {}^4\Sigma^-(a)$	
B	0.50753	0.50722	0.52659	0.52643	B	0.51679(45)
D	4.24×10^{-7}	1.01×10^{-7}	5.42×10^{-7}	7.74×10^{-7}	D	$4.92(11)\times10^{-7}$
p	2.0407	2.0360	1.52×10^{-3}	4.94×10^{-3}	λ	21.466(8)
p_J	2.15×10^{-4}	2.01×10^{-4}	-2.18×10^{-4}	-2.04×10^{-4}	γ	0.0109(20)
p_{JJ}	3.1×10^{-8}	2.4×10^{-8}	-3.3×10^{-8}	-2.6×10^{-8}	λ_J	$-7.1(15)\times10^{-6}$
$\hat{\sigma}$ (p, p_J and p_{JJ})	6.7×10^{-5}	9.4×10^{-5}	1.7×10^{-4}	1.4×10^{-4}	$\hat{\sigma}$	0.017
$\hat{\sigma}$ (B and D)	5.1×10^{-4}	2.5×10^{-3}	8.5×10^{-4}	2.7×10^{-3}		

The observed lambda doubling, $\Delta\nu_\Omega^{EXP}(J) = F'_{\Omega,e}(J) - F'_{\Omega,f}(J)$, of the $^4\Pi_{-1/2}$, $^4\Pi_{1/2}$, and $^4\Pi_{3/2}$ substates is shown in Fig. 4. There is no observable splitting of the $^4\Pi_{5/2}$ substate. According to the Budo and Kovacs formulae (*28*), the splitting of the $-1/2$ substate is negative and is proportional to J. The splitting of the $1/2$ substate is positive, is also proportional to J, and is comparable in magnitude to that of the $-1/2$ substate. The splittings of the $3/2$ and $5/2$ substates are much smaller and are proportional to J^3 and J^5, respectively. An attempt was made to fit the observed lambda doubling of the four substates to the Budo and Kovacs expressions. These expressions involve the constants C_i ($i = 0, 1, 2$) together with Y ($= A/B$) and were evaluated from fits to combination relations (A4), i.e., since $\Delta\nu_\Omega(J) = F'_{\Omega,e}(J) - F'_{\Omega,f}(J)$.

$$\frac{\Delta_1^q F'_{-1/2}(J) - \Delta_1^b F'_{-1/2}(J)}{4(J+1)} = -\frac{\sqrt{3}C_0}{Y+2}$$

$$\frac{\Delta_1^q F'_{1/2}(J) - \Delta_1^b F'_{1/2}(J)}{4(J+1)} = \frac{\sqrt{3}C_0 + C_1(Y+2)}{Y+2}$$

$$\frac{\Delta_1^q F'_{3/2}(J) - \Delta_1^b F'_{3/2}(J)}{4(J+1)} = \frac{2\sqrt{3}C_0 + C_1(7Y-6) + 2C_2Y(Y-2)}{Y(Y-2)^2} \times \left(J+\frac{1}{2}\right)\left(J+\frac{3}{2}\right)$$

$$\frac{\Delta_1^q F'_{5/2}(J) - \Delta_1^b F'_{5/2}(J)}{4(J+1)} = \frac{\sqrt{3}C_0 + 6C_1(Y-3) + 4C_2(Y-3)(Y-4)}{(Y-2)(Y-4)^2(Y-6)^2} \times \left(J-\frac{1}{2}\right)\left(J+\frac{1}{2}\right)\left(J+\frac{3}{2}\right)\left(J+\frac{5}{2}\right) \quad (10)$$

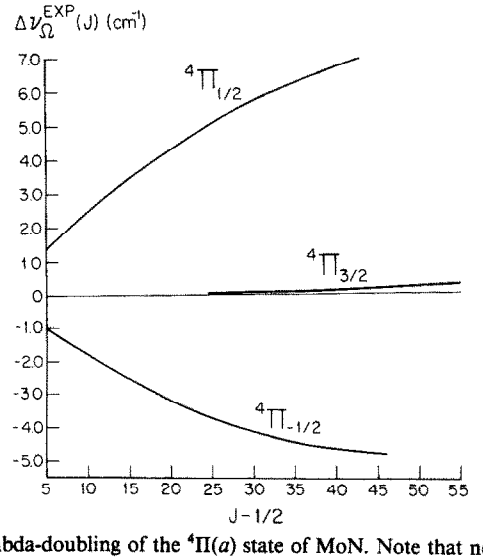

FIG. 4. The observed lambda-doubling of the $^4\Pi(a)$ state of MoN. Note that no doubling was observed for $^4\Pi_{5/2}$ and that this, therefore, is not included in the figure.

All four substates were included in the fit, which was carried out using the program MARQ (*29*), which utilizes Marquardt's method of nonlinear least squares (*30*). The results, which are presented in Table VI, are poor. The differences between calculated and observed combination differences exceed 100% for large values of J. The value of Y, which yields $A_v \sim 220$ cm^{-1}, is at least of the correct order of magnitude. A repeat of the fit in which the $^4\Pi_{5/2}$ substate was omitted produced even worse results. This discrepancy is not surprising however, since, as shown in Fig. 4, the observed splittings are not in agreement with the Budo–Kovacs predictions.

The Intermediate Analysis: $^4\Pi_\Omega \rightarrow {}^4\Sigma^-(a)$

The molecular constants B, D, λ, γ, and λ_J for the $^4\Sigma^-(a)$ state were obtained by using program MARQ to perform a nonlinear least-squares fit of sums and differences of the eigenvalues of the $^4\Sigma^-$ matrix (Table III) to observed combination differences. (γ_1 is placed equal to γ_2, and both are denoted by γ.) According to Eqs. (A1) and (A2), for each $^4\Sigma^-_\Omega$ substate:

$$\frac{\Delta_1^q F''_\Omega(J) + \Delta_1^b F''_\Omega(J)}{2} = F''_{\Omega,f}(J) + F''_{\Omega,f}(J+1) - F''_{\Omega,e}(J) - F''_{\Omega,e}(J+1) \qquad (11)$$

A total of 153 combination differences, encompassing all four $^4\Pi_\Omega \rightarrow {}^4\Sigma^-_\Omega$ subbands, were included in the fit. The values of the $^4\Sigma^-(a)$ constants which resulted are given in Table V.

Figure 5 is the theoretical spin-splitting diagram of the $^4\Sigma^-$ $v = 0$ state of MoN. The calculated term values, $F''_i(N)$, minus the purely rotational energy, $B''N(N+1) - D''N^2(N+1)^2$, are plotted against N. The term values are the eigenvalues of the $^4\Sigma^-$ matrix (Table III), using the molecular constants in Table V. The usual relationships hold between the F''_i, N, and J, i.e., F''_1: $J = N + 3/2 \cdots F''_4$: $J = N - 3/2$.

Figure 5 shows the transition of the $^4\Sigma^-$ state from Hund's case (a) to case (b) as N increases beyond $\sim$75. A $^4\Sigma$ state is better represented by a case (a) basis than by a case (b) basis when $|4\lambda| > \sqrt{3}BJ$ (*16*). A case (a) state comprises two substates, $^4\Sigma_{1/2}$ and $^4\Sigma_{3/2}$, which are separated in energy at low values of J by 4λ.

TABLE VI

Lambda-Doubling Constants for the $^4\Pi$ State Obtained by Fitting Combination Differences to the Formulae of Budo and Kovacs (cm^{-1})

Y	425*
C_0	31
C_1	0.034
C_2	-4.3×10^{-4}

*Y = A/B

As was shown above, the line frequencies calculated using the molecular constants obtained from combination differences disagree markedly with the measured frequencies at large values of J. Therefore, improved sets of constants for the $^4\Pi_\Omega$ substates were obtained by using MARQ to fit differences between calculated $^4\Pi_\Omega$ and $^4\Sigma^-(a)$ rotational levels directly to the corresponding frequencies. The $^4\Pi_\Omega$ energy level expressions used are the same as before, i.e., Eq. (8), but the $^4\Sigma^-(a)$ formulae are now the matrix eigenvalues (Table III). In addition, the $^4\Sigma^-(a)$ constants are not allowed to vary during the fit, but, instead, are fixed to the values in Table V. The reason for this is that the $^4\Sigma^-(a)$ eigenvalues are derived using a very accurate Hamiltonian, Eq. (3), whereas the $^4\Pi_\Omega$ expressions, Eq. (8), are very simplistic.

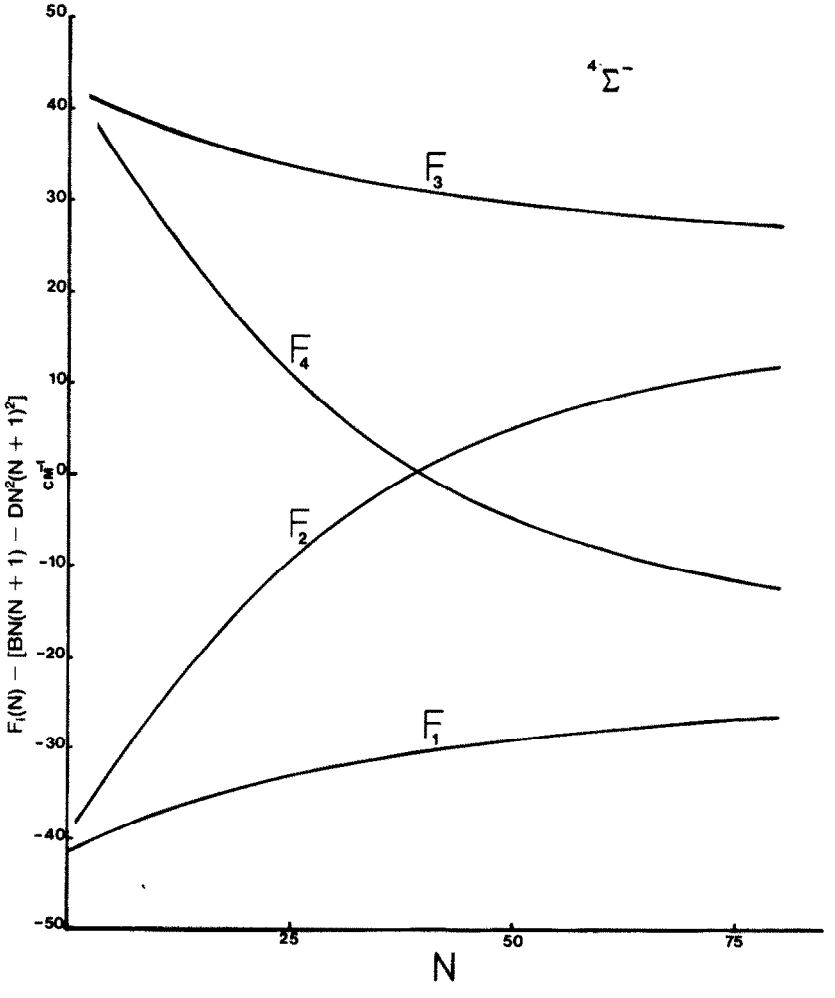

FIG. 5. Theoretical spin splitting diagram for the $^4\Sigma^-(a)$ $v = 0$ state. Note that the figure has been drawn to correspond to the calculated levels for the $^4\Sigma^-(a)$ state of MoN.

MARQ is used to fit the differences between the rotational levels of the $^4\Pi_\Omega$ and $^4\Sigma^-_\Omega$ substates to the measured frequencies of each subband to obtain B'_Ω, D'_Ω, p'_Ω, $p'_{J,\Omega}$, and $p'_{JJ,\Omega}$. The results are summarized in Table VII. The fits for the $^4\Pi_{3/2} \rightarrow {}^4\Sigma^-_{1/2}$ and $^4\Pi_{5/2} \rightarrow {}^4\Sigma^-_{3/2}$ subbands are extremely good, as can be seen from the values of the standard deviations ($\sim$0.01 cm^{-1}). In fact, the maximum deviation between measured and calculated frequencies is $\approx$0.03 cm^{-1}. The fits for the $^4\Pi_{1/2} \rightarrow {}^4\Sigma^-_{1/2}$ and $^4\Pi_{-1/2} \rightarrow {}^4\Sigma^-_{3/2}$ subbands are not quite as good; the standard deviations are $\approx$0.04 cm^{-1}. In the latter two subbands, there are branches whose calculated frequencies differ from the measured values by as much as 0.20 cm^{-1} for values of J between 55.5 and 60.5.

The Concerted Analysis: $^4\Pi(a) \rightarrow {}^4\Sigma^-(a)$

The molecular constants for the $^4\Pi$ state taken as a whole are obtained from the "direct" nonlinear least-squares fitting procedure of Zare *et al.* (*20*). In this procedure the Hamiltonian matrices of the upper and lower electronic states are numerically diagonalized, and the differences between the eigenvalues are fitted directly to the corresponding measured line frequencies. This approach allows all the observed lines (except those deliberately rejected) to be included in the fit, regardless of how fragmentary a given branch may be. A program named DIRECT was written to calculate the $^4\Pi$ constants by calling MARQ to perform the fit.

In the case of a $^4\Sigma^-(a)$ state it is not necessary to numerically diagonalize the Hamiltonian matrix, since, in the case (a) parity basis set (4), it reduces to two 2×2 matrices. DIRECT first calculates the $^4\Sigma^-$ eigenvalues, $F''_{\Omega,e}(J)$ and $F''_{\Omega,f}(J)$, using the $^4\Sigma^-(a)$ molecular constants, obtained from the combination relations, in Table V. As in the previous calculation, these eigenvalues remain unchanged during the fit, i.e., the $^4\Sigma^-(a)$ constants are not varied by MARQ. In view of the strong perturbations acting upon the $^4\Pi$ state, it was thought worthwhile to omit the spin–orbit splitting constant, A, altogether. This was accomplished by fixing the value of A to zero during the fit. The $^4\Pi$ constants which result are given in Table VIII.

TABLE VII

Molecular Constants for the $^4\Pi_\Omega$ Substates Obtained from Least-Squares Fits Directly to the Frequencies of Each Subband (cm^{-1}) [The lower state used is the $^4\Sigma^-$ matrix (Table III) with fixed values of the $^4\Sigma^-$ constants (Table V)]*

Substates	B	D	p	p_J	p_{JJ}	$\hat{\sigma}$
$^4\Pi_{-1/2}$	0.49360(1)	$-1.49(3)\times10^{-7}$	-0.16974(39)	$-4.21(6)\times10^{-5}$	$-4.61(24)\times10^{-9}$	0.041
$^4\Pi_{1/2}$	0.50995(1)	$9.47(1)\times10^{-7}$	0.22438(32)	$4.57(3)\times10^{-5}$	$5.55(8)\times10^{-9}$	0.041
$^4\Pi_{3/2}$	0.50506(1)	$5.13(1)\times10^{-7}$	$4.4(31)\times10^{-4}$	$-1.3(3)\times10^{-6}$	$-1.9(80)\times10^{-11}$	0.012
$^4\Pi_{5/2}$	0.50591(1)	$4.79(1)\times10^{-7}$				0.009

*The uncertainties listed in this table do not include any contribution from the constants of the quartet sigma (ground) state. Inclusion of them increases the magnitude of the uncertainties by about an additional factor of two.

TABLE VIII

$^4\Pi$ Constants Obtained from a Least-Squares Fit Directly to the Frequencies of the 0, 0 Band (All constants in cm^{-1})

$T_{-1/2}$	15,898.84
$T_{1/2}$	15,963.26
$T_{3/2}$	16,282.73
$T_{5/2}$	16,718.48
A	0.0 (fixed)
B	0.50380
ε	-0.152655
α	2.0096
p	0.025970
q	-1.9445×10^{-4}
γ	0.074130
A_D	4.0295×10^{-4}
D	4.8072×10^{-7}
$\hat{G}$	0.11

The standard deviation of the fit is $\sim 0.10\ cm^{-1}$, and the differences between the measured and calculated frequencies vary from ~ 0.01 to $0.6\ cm^{-1}$. As is noted in the next section, nearly all of the discrepancies arise from the failure of the perturbation Hamiltonian H_Λ to describe the lambda doubling of the $^4\Pi_{3/2}$ substate.

DISCUSSION

The remaining problems in the analysis of the MoN spectrum are: (i) Deciding the functional forms of the corrections to the diagonal elements of the $^4\Pi$ matrices. The constants in Table VIII are calculated using only an empirical parameter, T_Ω, which is adjusted during the fitting in order to absorb the effects of the perturbations. (ii) Deriving corrections to the Hamiltonian for the lambda-doubling interaction, H_Λ, which, as it stands, fails to predict the lambda doubling observed in the $^4\Pi_{3/2}$ substate.

In order to shed light on these problems the eigenvalues of the $^4\Pi$ matrices, which are calculated by DIRECT, were compared with experimental values of the $^4\Pi$ rotational energy levels. It is not possible in general to determine absolute experimental values of the rotational levels; one can only measure their differences, i.e., the frequencies. However, for the $^4\Pi(a) \rightarrow {}^4\Sigma^-(a)$ transition in MoN, this can be resolved by calculating "experimental" rotational levels for the $^4\Pi$ state, which do not depend upon any theoretical model of that state and which include the

electronic and vibrational energy, ${}^eT_0$, of the state. These are denoted $T'_{\Omega,e}(J)$ and $T'_{\Omega,f}(J)$ and are given by Eqs. (12) and (13);

$$T'_{\Omega,e}(J) = 1/3[F''_{\Omega,e}(J-1) + F''_{\Omega,f}(J) + F''_{\Omega,e}(J+1) + P_{ee,\Omega}(J+1) + Q_{ef,\Omega}(J) + R_{ee,\Omega}(J-1)] \quad (12)$$

$$T'_{\Omega,f}(J) = 1/3[F''_{\Omega,f}(J-1) + F''_{\Omega,e}(J) + F''_{\Omega,f}(J+1) + P_{ff,\Omega}(J+1) + Q_{fe,\Omega}(J) + R_{ff,\Omega}(J-1)]. \quad (13)$$

The matrix isolation studies of Bates and Gruen (*13*) and Knight and Steadman (*14*) indicate that the ${}^4\Sigma^-$ state is the ground state of MoN. The calculated rotational levels of the ${}^4\Sigma^-$ state are then simply the eigenvalues, $F''_{\Omega,e}(J)$ and $F''_{\Omega,f}(J)$, of the

TABLE IXa

"Experimental" and Calculated ${}^4\Pi_{-1/2}$ Rotational Energy Levels (cm^{-1})

	E LEVELS			F LEVELS		
J	EXPTL.	CALCD.	DIFF.	EXPTL.	CALCD.	DIFF.
2.5	15902.650	15902.696	-0.046	15903.172	15903.214	-0.042
3.5	906.022	906.063	-0.041	906.717	906.752	-0.035
4.5	910.388	910.417	-0.029	911.231	911.276	-0.045
5.5	915.709	915.759	-0.050	916.754	916.785	-0.031
6.5	922.030	922.088	-0.058	923.239	923.280	-0.041
7.5	929.348	929.405	-0.057	930.727	930.761	-0.034
8.5	937.652	937.710	-0.058	939.198	939.227	-0.029
9.5	946.960	947.003	-0.043	948.654	948.679	-0.025
10.5	957.237	957.285	-0.048	959.079	959.116	-0.037
11.5	968.496	968.556	-0.060	970.510	970.539	-0.029
12.5	980.759	980.816	-0.057	982.915	982.948	-0.033
13.5	994.001	994.065	-0.064	996.306	996.342	-0.036
14.5	16008.248	16008.304	-0.056	16010.692	16010.722	-0.030
15.5	023.490	023.533	-0.043	026.058	026.088	-0.030
16.5	039.707	039.751	-0.044	042.418	042.440	-0.022
17.5	056.916	056.960	-0.044	059.756	059.778	-0.022
18.5	075.116	075.159	-0.043	078.092	078.102	-0.010
19.5	094.332	094.348	-0.016	097.401	097.413	-0.012
20.5	114.507	114.529	-0.022	117.698	117.709	-0.011
21.5	135.687	135.700	-0.013	138.985	138.992	-0.007
22.5	157.857	157.862	-0.005	161.253	161.262	-0.009
23.5	181.000	181.015	-0.015	184.514	184.519	-0.005
24.5	205.140	205.159	-0.019	208.754	208.762	-0.008
25.5	230.290	230.295	-0.005	234.000	233.992	0.008
26.5	256.429	256.421	0.008	260.214	260.209	0.005
27.5	283.549	283.539	0.010	287.421	287.414	0.007
28.5	311.657	311.649	0.008	315.613	315.605	0.008
29.5	340.768	340.749	0.019	344.790	344.784	0.006
30.5	370.864	370.841	0.023	374.967	374.950	0.017
31.5	401.933	401.924	0.009	406.121	406.103	0.018
32.5	434.028	433.999	0.029	438.264	438.243	0.021
33.5	467.097	467.064	0.033	471.407	471.371	0.036
34.5	501.160	501.120	0.040	505.510	505.486	0.024
35.5	536.217	536.167	0.050	540.631	540.598	0.043
36.5	572.241	572.205	0.036	576.701	576.678	0.023
37.5	609.304	609.234	0.070	613.791	613.755	0.036
38.5	647.324	647.253	0.071	651.867	651.818	0.049
39.5	686.347	686.261	0.086	690.900	690.869	0.031
40.5	726.336	726.260	0.076	730.946	730.906	0.040
41.5	767.293	767.249	0.044	771.964	771.930	0.034
42.5	809.306	809.227	0.079	813.980	813.941	0.039
43.5	852.268	852.194	0.074	856.996	856.937	0.059
44.5	896.229	896.150	0.079	900.965	900.920	0.045
45.5	941.171	941.094	0.077	945.919	945.889	0.030
46.5	987.048	987.027	0.021	991.869	991.843	0.026

$^4\Sigma^-$ matrices. Thus, Eqs. (12) and (13) yield the "experimental" rotational energy levels, $T'_{\Omega,e}(J)$ and $T'_{\Omega,f}(J)$, of the $^4\Pi$ state by adding the appropriate measured line frequencies to $F''_{\Omega,e}(J)$ and $F''_{\Omega,f}(J)$. The calculated $^4\Pi$ rotational levels are obtained from the values of T_Ω (Table VIII) and the eigenvalues, $F'_{\Omega,e}(J)$ and $F'_{\Omega,f}(J)$, of the $^4\Pi$ matrices. These calculated and "experimental" $^4\Pi$ rotational levels and their differences are given in Table IX for each $^4\Pi_\Omega$ substate.

The calculated lambda doubling for each substate, $\Delta\nu_\Omega^{CALC}(J)$ is, by definition, equal to $F'_{\Omega,e}(J) - F'_{\Omega,f}(J)$. The "experimental" lambda doubling $T'_{\Omega,e}(J) - T'_{\Omega,f}(J)$. Both lambda doublings are given in Table X. From Table X we see at once that the calculated lambda doubling of the $^4\Pi_{3/2}$ substate is much smaller than the observed. On the other hand, H_A predicts the lambda doubling of the other three substates quite satisfactorily. The two tables show clearly where the calculated and "experimental" $^4\Pi$ levels differ.

The results given here indicate that a much more satisfactory theoretical formula for H_A is needed to adequately describe the lambda doubling of the $^4\Pi_{3/2}$ substate.

TABLE IXb

"Experimental" and Calculated $^4\Pi_{1/2}$ Rotational Energy Levels (cm^{-1})

	E LEVELS			F LEVELS		
J	EXPTL.	CALCD.	DIFF.	EXPTL.	CALCD.	DIFF.
3.5	15973.838	15973.793	0.045	15972.916	15972.899	0.017
4.5	978.530	978.498	0.032	977.402	977.384	0.018
5.5	984.277	984.223	0.054	982.879	982.890	-0.011
6.5	991.021	990.967	0.054	989.405	989.417	-0.012
7.5	998.766	998.731	0.035	996.946	996.966	-0.020
8.5	16007.561	16007.513	0.048	16005.509	16005.536	-0.027
9.5	017.354	017.314	0.040	015.082	015.127	-0.045
10.5	028.168	028.132	0.036	025.702	025.739	-0.037
11.5	039.999	039.968	0.031	037.315	037.371	-0.056
12.5	052.845	052.820	0.025	049.965	050.024	-0.059
13.5	066.702	066.689	0.013	063.623	063.696	-0.073
14.5	081.581	081.574	0.007	078.302	078.389	-0.087
15.5	097.476	097.474	0.002	094.017	094.100	-0.083
16.5	114.382	114.388	-0.006	110.742	110.830	-0.088
17.5	132.299	132.317	-0.018	128.489	128.578	-0.089
18.5	151.231	151.259	-0.028	147.245	147.344	-0.099
19.5	171.184	171.214	-0.030	167.036	167.128	-0.092
20.5	192.143	192.181	-0.038	187.832	187.928	-0.096
21.5	214.118	214.160	-0.042	209.635	209.744	-0.109
22.5	237.103	237.151	-0.048	232.477	232.575	-0.098
23.5	261.099	261.151	-0.052	256.329	256.421	-0.092
24.5	286.104	286.162	-0.058	281.183	281.282	-0.099
25.5	312.124	312.181	-0.057	307.056	307.156	-0.100
26.5	339.152	339.210	-0.058	333.936	334.043	-0.107
27.5	367.182	367.246	-0.064	361.854	361.942	-0.088
28.5	396.228	396.290	-0.062	390.780	390.852	-0.072
29.5	426.278	426.340	-0.062	420.696	420.774	-0.078
30.5	457.336	457.396	-0.060	451.638	451.705	-0.067
31.5	489.400	489.458	-0.058	483.574	483.646	-0.072
32.5	6522.476	522.525	-0.049	516.543	516.596	-0.053
33.5	556.547	556.595	-0.048	550.510	550.553	-0.043
34.5	591.631	591.670	-0.039	585.495	585.518	-0.023
35.5	627.700	627.746	-0.046	621.475	621.489	-0.014
36.5	664.790	664.825	-0.035	658.473	658.465	0.008
37.5	702.877	702.906	-0.029	696.461	696.447	0.014
38.5	741.964	741.987	-0.023	735.462	735.433	0.029
39.5	782.061	782.069	-0.008	775.461	775.422	0.039
40.5	823.145	823.150	-0.005	816.463	816.414	0.049
41.5	865.225	865.229	-0.004	858.474	858.407	0.067
42.5	908.323	908.307	0.016	901.485	901.402	0.083
43.5	952.415	952.382	0.033	945.478	945.397	0.081

TABLE IXc

"Experimental" and Calculated $^4\Pi_{3/2}$ Rotational Energy Levels (cm^{-1})

	E LEVELS			F LEVELS		
J	EXPTL.	CALCD.	DIFF.	EXPTL.	CALCD.	DIFF.
3.5	16291.781	16291.596	0.185	16291.773	16291.596	0.177
4.5	296.319	296.142	0.177	296.318	296.142	0.176
5.5	301.872	301.699	0.173	301.877	301.699	0.178
6.5	308.438	308.265	0.173	308.440	308.265	0.175
7.5	316.013	315.842	0.171	316.013	315.842	0.171
8.5	324.599	324.428	0.171	324.591	324.428	0.163
9.5	334.195	334.025	0.170	334.183	334.024	0.159
10.5	344.801	344.630	0.171	344.794	344.630	0.164
11.5	356.409	356.246	0.163	356.403	356.246	0.157
12.5	369.034	368.871	0.163	369.028	368.871	0.157
13.5	382.667	382.506	0.161	382.660	382.505	0.155
14.5	397.307	397.149	0.158	397.303	397.149	0.154
15.5	412.953	412.802	0.151	412.951	412.801	0.150
16.5	429.609	429.463	0.146	429.594	429.462	0.132
17.5	447.282	447.133	0.149	447.266	447.132	0.134
18.5	465.959	465.811	0.148	465.953	465.811	0.142
19.5	485.636	485.498	0.138	485.620	485.497	0.123
20.5	506.330	506.193	0.137	506.311	506.191	0.120
21.5	528.030	527.895	0.135	527.998	527.894	0.104
22.5	550.735	550.605	0.130	550.710	550.603	0.107
23.5	574.449	574.322	0.127	574.423	574.320	0.103
24.5	599.166	599.045	0.121	599.126	599.044	0.082
25.5	624.890	624.776	0.114	624.860	624.774	0.086
26.5	651.624	651.513	0.111	651.587	651.511	0.076
27.5	679.365	679.256	0.109	679.324	679.253	0.071
28.5	708.106	708.005	0.101	708.032	708.002	0.030
29.5	737.851	737.759	0.092	737.811	737.756	0.055
30.5	768.609	768.518	0.091	768.554	768.514	0.040
31.5	800.358	800.282	0.076	800.309	800.278	0.031
32.5	833.126	833.050	0.076	833.064	833.046	0.018
33.5	866.889	866.822	0.067	866.816	866.817	-0.001
34.5	901.656	901.598	0.058	901.586	901.593	-0.007
35.5	937.427	937.376	0.051	937.357	937.371	-0.014
36.5	974.199	974.158	0.041	974.118	974.152	-0.034
37.5	17011.976	17011.942	0.034	17011.885	17011.935	-0.050
38.5	050.750	050.727	0.023	050.653	050.721	-0.068
39.5	090.527	090.514	0.013	090.426	090.507	-0.081
40.5	131.300	131.302	-0.002	131.191	131.295	-0.104
41.5	173.079	173.091	-0.012	172.949	173.082	-0.133
42.5	215.856	215.879	-0.023	215.734	215.870	-0.136
43.5	259.630	259.667	-0.037	259.503	259.658	-0.155
44.5	304.406	304.454	-0.048	304.268	304.444	-0.176
45.5	350.178	350.240	-0.062	350.031	350.229	-0.198
46.5	396.941	397.023	-0.082	396.790	397.011	-0.221
47.5	444.710	444.803	-0.093	444.550	444.791	-0.241
48.5	493.472	493.581	-0.109	493.299	493.568	-0.269
49.5	543.228	543.355	-0.127	543.052	543.341	-0.289
50.5	593.981	594.124	-0.143	593.794	594.110	-0.316
51.5	645.738	645.889	-0.151	645.524	645.873	-0.349
52.5	698.464	698.648	-0.184	698.262	698.631	-0.369
53.5	752.196	752.400	-0.204	751.986	752.383	-0.397
54.5	806.921	807.146	-0.225	806.687	807.128	-0.441
55.5	862.642	862.885	-0.243	862.372	862.866	-0.494
56.5	919.354	919.616	-0.262	919.083	919.596	-0.513

The way in which the strong central features (Fig. 2b in particular) depend very subtly upon this has already been noted. Changing H_A will produce changes in the values of some of the diagonal *and* off-diagonal elements in Table II. Corrections will then need to be made to the T_Ω in order to improve the fit still further and consequently improve the values of the $^4\Pi$ molecular constants. This work is now being undertaken.

TABLE IXd

"Experimental" and Calculated $^4\Pi_{5/2}$ Rotational Energy Levels (cm^{-1})

	E LEVELS			F LEVELS		
J	EXPTL.	CALCD.	DIFF.	EXPTL.	CALCD.	DIFF.
7.5	16747.791	16747.872	-0.081	16747.794	16747.872	-0.078
8.5	756.386	756.470	-0.084	756.388	756.470	-0.082
9.5	766.000	766.080	-0.080	766.008	766.080	-0.072
10.5	776.621	776.701	-0.080	776.631	776.701	-0.070
11.5	788.254	788.333	-0.079	788.261	788.333	-0.072
12.5	800.898	800.976	-0.078	800.907	800.976	-0.069
13.5	814.556	814.629	-0.073	814.555	814.629	-0.074
14.5	829.227	829.293	-0.066	829.221	829.293	-0.072
15.5	844.896	844.968	-0.072	844.897	844.968	-0.071
16.5	861.576	861.653	-0.077	861.581	861.653	-0.072
17.5	879.278	879.348	-0.070	879.281	879.348	-0.067
18.5	897.976	898.052	-0.076	897.976	898.052	-0.076
19.5	917.703	917.766	-0.063	917.704	917.766	-0.062
20.5	938.421	938.490	-0.069	938.421	938.490	-0.069
21.5	960.160	960.223	-0.063	960.162	960.223	-0.061
22.5	982.912	982.964	-0.052	982.901	982.964	-0.063
23.5	17006.661	17006.714	-0.053	17006.657	17006.715	-0.058
24.5	031.427	031.473	-0.046	031.419	031.473	-0.054
25.5	057.194	057.240	-0.046	057.183	057.240	-0.057
26.5	083.970	084.014	-0.044	083.962	084.014	-0.052
27.5	111.720	111.796	-0.076	111.754	111.796	-0.042
28.5	140.545	140.585	-0.040	140.542	140.585	-0.043
29.5	170.340	170.381	-0.041	170.344	170.381	-0.037
30.5	201.150	201.183	-0.033	201.147	201.183	-0.036
31.5	232.969	232.991	-0.022	232.953	232.991	-0.038
32.5	265.781	265.805	-0.024	265.779	265.805	-0.026
33.5	299.604	299.624	-0.020	299.602	299.624	-0.022
34.5	334.434	334.449	-0.015	334.435	334.449	-0.014
35.5	370.256	370.277	-0.021	370.270	370.277	-0.007
36.5	407.098	407.110	-0.012	407.103	407.110	-0.007
37.5	444.944	444.947	-0.003	444.947	444.947	0.000
38.5	483.795	483.787	0.008	483.791	483.787	0.004
39.5	523.639	523.629	0.010	523.639	523.629	0.010
40.5	564.486	564.474	0.012	564.491	564.474	0.017
41.5	606.342	606.321	0.021	606.340	606.321	0.019
42.5	649.200	649.169	0.031	649.202	649.169	0.033
43.5	693.054	693.018	0.036	693.049	693.018	0.031
44.5	737.902	737.867	0.035	737.915	737.868	0.047
45.5	783.773	783.717	0.056	783.771	783.717	0.054
46.5	830.634	830.565	0.069	830.628	830.566	0.062
47.5	878.465	878.412	0.053	878.478	878.413	0.065
48.5	927.325	927.258	0.067	927.324	927.258	0.066
49.5	977.182	977.101	0.081	977.178	977.101	0.077
50.5	18028.035	18027.941	0.094	18028.033	18027.941	0.092

CONCLUSIONS

The red system of MoN is undoubtedly a $^4\Pi(a) \rightarrow {}^4\Sigma^-(a)$ transition despite some problems in the agreement between the experimental and theoretical energy levels. The most surprising aspect of the $^4\Pi$ state is the significant displacement of the $\Omega = -1/2$ component from the position expected for reasonable case (a) behavior. Even allowing for spin uncoupling, the level is shifted ~ 175 cm^{-1} from its "expected" position and yet there is no evidence of rotational perturbations in this, or in any other, component. The inability of the present theoretical framework to correctly account for the Λ doubling of the $\Omega = 3/2$ component, together with the shift of the $\Omega = -1/2$ component, suggests either—or both—of a perturbation by a non-$^4\Sigma$ state ($^2\Pi$?) or the effects of uncoupling toward case d. Despite the inherent plausibility of this latter, since the $p\pi$ electron has much of a Rydberg character

TABLE X

"Experimental" and Calculated Lambda-Doubling of the $^4\Pi$ State (cm^{-1})

	$^4\Pi_{-1/2}$			$^4\Pi_{1/2}$	
J	EXPTL.	CALCD.	J	EXPTL.	CALCD.
2.5	-0.522	-0.518	3.5	0.922	0.893
3.5	-0.695	-0.689	4.5	1.128	1.114
4.5	-0.843	-0.858	5.5	1.398	1.333
6.5	-1.209	-1.192	7.5	1.820	1.765
5.5	-1.045	-1.026	6.5	1.616	1.550
7.5	-1.379	-1.356	8.5	2.052	1.978
8.5	-1.546	-1.517	9.5	2.272	2.187
9.5	-1.694	-1.676	10.5	2.466	2.394
10.5	-1.842	-1.831	11.5	2.684	2.597
11.5	-2.014	-1.983	12.5	2.880	2.797
12.5	-2.156	-2.132	13.5	3.079	2.993
13.5	-2.305	-2.277	14.5	3.279	3.185
14.5	-2.444	-2.418	15.5	3.459	3.374
15.5	-2.568	-2.556	16.5	3.640	3.558
16.5	-2.711	-2.689	17.5	3.810	3.739
17.5	-2.840	-2.818	18.5	3.986	3.915
18.5	-2.976	-2.943	19.5	4.148	4.086
19.5	-3.069	-3.064	20.5	4.311	4.254
20.5	-3.191	-3.181	21.5	4.483	4.417
21.5	-3.298	-3.293	22.5	4.626	4.576
22.5	-3.396	-3.400	23.5	4.770	4.730
23.5	-3.514	-3.504	24.5	4.921	4.880
24.5	-3.614	-3.603	25.5	5.068	5.026
25.5	-3.710	-3.698	26.5	5.216	5.167
26.5	-3.785	-3.788	27.5	5.328	5.304
27.5	-3.872	-3.874	28.5	5.448	5.437
28.5	-3.956	-3.956	29.5	5.582	5.566
29.5	-4.022	-4.034	30.5	5.698	5.691
30.5	-4.103	-4.109	31.5	5.826	5.812
31.5	-4.188	-4.179	32.5	5.933	5.929
32.5	-4.236	-4.245	33.5	6.037	6.042
33.5	-4.310	-4.307	34.5	6.136	6.152
34.5	-4.350	-4.366	35.5	6.225	6.258
35.5	-4.414	-4.421	36.5	6.317	6.360
36.5	-4.460	-4.473	37.5	6.416	6.459
37.5	-4.487	-4.521	38.5	6.502	6.554
38.5	-4.543	-4.566	39.5	6.600	6.647
39.5	-4.553	-4.607	40.5	6.682	6.736
40.5	-4.610	-4.646	41.5	6.751	6.822
41.5	-4.671	-4.681	42.5	6.838	6.905
42.5	-4.674	-4.714	43.5	6.937	6.985
43.5	-4.728	-4.743			
44.5	-4.736	-4.770			
45.5	-4.748	-4.794			
46.5	-4.821	-4.816			

(*vide infra*), preliminary calculations do not bear out this interpretation and the origin of the Λ doubling and spin–orbit discrepancies remain unattributed.

The magnitude of the zero-field splitting of the $^4\Sigma^-$ state is extremely large and affords an excellent example of a "case (a)" $^4\Sigma^-$ state. This splitting indicates the importance of higher-order spin–orbit effects in the second-row transition elements and the importance of intermediate coupling for molecules containing these atoms.

The combination of the very small change in the upper- and lower-state B values (of the order of 3.5%), the magnitude of the spin–orbit coupling constant, and the characterization of the ground state as $^4\Sigma^-$ unambiguously assign this transition as highly localized upon the metal atom and of a pseudoligand-field type (*31–33*). Even though it is not correct to describe the molecule as $Mo^{3+}N^{3-}$, nonetheless the preponderant configuration for the ground term (*34*) is undoubtedly $s\sigma^1 d\delta^2$. Similarly, it seems clear from the intensity of the transition that the excited state configuration is predominantly $d\delta^2 p\pi^1$, where the $p\pi$ orbital is the Van Vleck "pure precession"

TABLE X—*Continued*

	$^4\Pi_{3/2}$			$^4\Pi_{5/2}$	
J	EXPTL.	CALCD.	J	EXPTL.	CALCD.
3.5	0.008	0.000	7.5	-0.003	-0.000
4.5	0.001	0.000	8.5	-0.002	-0.000
5.5	-0.005	0.000	9.5	-0.008	-0.000
6.5	-0.002	0.000	10.5	-0.010	-0.000
7.5	0.000	0.000	11.5	-0.007	-0.000
8.5	0.008	0.000	12.5	-0.009	-0.000
9.5	0.012	0.000	13.5	0.001	-0.000
10.5	0.007	0.000	14.5	0.006	-0.000
11.5	0.006	0.000	15.5	-0.001	-0.000
12.5	0.006	0.000	16.5	-0.005	-0.000
13.5	0.007	0.000	17.5	-0.003	-0.000
14.5	0.004	0.000	18.5	0.000	-0.000
15.5	0.002	0.000	19.5	-0.001	-0.000
16.5	0.015	0.001	20.5	0.000	-0.000
17.5	0.016	0.001	21.5	-0.002	-0.000
18.5	0.006	0.001	22.5	0.011	-0.000
19.5	0.016	0.001	23.5	0.004	-0.000
20.5	0.019	0.001	24.5	0.008	-0.000
21.5	0.032	0.001	25.5	0.011	-0.000
22.5	0.025	0.001	26.5	0.008	-0.000
23.5	0.026	0.002	27.5	-0.004	-0.000
24.5	0.040	0.002	28.5	0.003	-0.000
25.5	0.030	0.002	29.5	-0.004	-0.000
26.5	0.037	0.002	30.5	0.003	-0.000
27.5	0.041	0.003	31.5	0.016	-0.000
28.5	0.074	0.003	32.5	0.002	-0.000
29.5	0.040	0.003	33.5	0.002	-0.000
30.5	0.055	0.003	34.5	-0.001	-0.000
31.5	0.049	0.004	35.5	-0.014	-0.000
32.5	0.062	0.004	36.5	-0.005	-0.000
33.5	0.073	0.005	37.5	-0.003	-0.000
34.5	0.070	0.005	38.5	0.004	-0.000
35.5	0.070	0.005	39.5	0.000	-0.000
36.5	0.081	0.006	40.5	-0.005	-0.000
37.5	0.091	0.006	41.5	0.002	-0.000
38.5	0.097	0.007	42.5	-0.002	-0.000
39.5	0.101	0.007	43.5	0.005	-0.000
40.5	0.109	0.008	44.5	-0.013	-0.000
41.5	0.130	0.008	45.5	0.002	-0.000
42.5	0.122	0.009	46.5	0.006	-0.000
43.5	0.127	0.010	47.5	-0.013	-0.000
44.5	0.138	0.010	48.5	0.001	-0.001
45.5	0.147	0.011	49.5	0.004	-0.001
46.5	0.151	0.012	50.5	0.002	-0.001
47.5	0.160	0.012			
48.5	0.173	0.013			
49.5	0.176	0.014			
50.5	0.187	0.015			
51.5	0.214	0.015			
52.5	0.202	0.016			
53.5	0.210	0.017			
54.5	0.234	0.018			
55.5	0.270	0.019			
56.5	0.271	0.020			

partner of a higher-lying $p\sigma$ (*35*), with both of these orbitals being, predominantly, the "Stark" components of the atomic $5p$ orbital essentially localized on the Mo atom. In this regard, it is the $5s\sigma \rightarrow 5p\pi$ analog of the $A \rightarrow X$ system of TiN (*1*), the $A \rightarrow X$ system of ZrN (*3*), the $A^3\Phi \rightarrow X^3\Delta$ system of NbN (*4*), a similar system in TaN (*9*), and all of the individual analogs of these transitions in the transition metal oxide species (ScO, TiO, VO, ZrO, NbO, etc.) (*31, 36*). A more systematic semiempirical approach to this series of assignments has been worked out (*37*) and will be published elsewhere.

The present MoN system has been seen (*13, 14*) in low temperatures in a matrix where, of course, only the $^4\Sigma^-_{1/2}$ component is populated. These spectra also suggest the presence of the one-electron analog $s\sigma \rightarrow p\sigma$ at higher energies, as is seen for many other species (*3, 38*) and there are, indeed, fragments of other systems to higher energies in the gas phase which have not yet been analyzed (*39*).

Finally, it seemed appropriate to search for the particularly strong, line-like, feature at 6123 Å in the spectra of M- and S-type stars. Despite a careful search, only one feature in the spectrum of β-Pegasi (*40*), an M-type star, was found at this wavelength. The feature was originally ascribed to TiO, but more recent spectra of TiO do not show any strong features at this precise wavelength. It is also interesting to note that the feature is given a precision in location of only about 0.5 Å compared with the 0.02 Å for many other features in this spectrum—thereby suggesting that it is not the usual kind of well-defined bandhead or atomic line. In the case of the red system of titanium nitride (*1*), most of the major bandheads are obscured by the prominent calcium principal series transition, but in molybdenum nitride these do not coincide. The precision of the present observations should be more than adequate to enable the red system of MoN to be identified in future stellar investigations.

APPENDIX: COMBINATION RELATIONS USED FOR THE PRELIMINARY AND INTERMEDIATE ANALYSES

Reference to Fig. 3 shows the following relations for the $^4\Sigma_\Omega^-$ substates

$$F''_f(J) - F''_e(J+1) = P_{ee}(J+1) - Q_{ef}(J) = Q_{fe}(J+1) - R_{ff}(J)$$

$$F''_f(J+1) - F''_e(J) = R_{ee}(J) - Q_{ef}(J+1) = Q_{fe}(J) - P_{ff}(J+1), \qquad \text{(A1)}$$

and, from these, the following combination relations for each $^4\Sigma_\Omega^-$ substate can be formed

$$\Delta_1^a F''(J) = R_{ee}(J) - Q_{ef}(J+1) + Q_{fe}(J) - P_{ff}(J+1)$$

$$\Delta_1^b F''(J) = P_{ee}(J+1) - Q_{ef}(J) + Q_{fe}(J+1) - R_{ff}(J). \qquad \text{(A2)}$$

Also by reference to Fig. 3 it can be seen that, for each $^4\Pi_\Omega$ substate,

$$F'_f(J+1) - F'_e(J) = Q_{fe}(J+1) - P_{ee}(J+1) = R_{ff}(J) - Q_{ef}(J)$$

$$F'_e(J+1) - F'_f(J) = Q_{ef}(J+1) - P_{ff}(J+1) = R_{ee}(J) - Q_{fe}(J), \qquad \text{(A3)}$$

and, accordingly,

$$\Delta_1^a F'(J) = Q_{ef}(J+1) - P_{ff}(J+1) + R_{ee}(J) - Q_{fe}(J)$$

$$\Delta_1^b F'(J) = Q_{fe}(J+1) - P_{ee}(J+1) + R_{ff}(J) - Q_{ef}(J). \qquad \text{(A4)}$$

ACKNOWLEDGMENTS

We gratefully acknowledge that this work was made possible by the award of Grant GP 16089 from the National Science Foundation to T.M.D. We also acknowledge valuable comments from Dr. R. W. Field, Dr. A. J. Merer, and Dr. S. P. Davis.

RECEIVED: May 25, 1984

REFERENCES

1. T. M. DUNN, L. K. HANSON, AND K. A. RUBINSON, *Canad. J. Phys.* **48**, 1657–1663 (1970).
2. J. K. BATES, N. L. RANIERI, AND T. M. DUNN, *Canda. J. Phys.* **54**, 915–916 (1976).

3. J. K. BATES AND T. M. DUNN, *Canad. J. Phys.* **54,** 1216–1223 (1976).
4. T. M. DUNN AND K. M. RAO, *Nature (London)* **222,** 266–267 (1969).
5. J.-L. FÉMÉNIAS, C. ATHÉNOUR, AND T. M. DUNN, *J. Chem. Phys.* **63,** 2861–2868 (1975).
6. J. C. HOWARD AND J. G. CONWAY, *J. Chem. Phys.* **43,** 3055–3057 (1965).
7. S. G. KRISHNAMURTI AND M. SWAMINATHAN, *Curr. Sci. (India)* **23,** 258–262 (1954).
8. M. MANDICH, J. K. BATES, AND T. M. DUNN, to be published.
9. J. K. BATES AND T. M. DUNN, to be published.
10. J. K. BATES AND T. M. DUNN, to be published.
11. J. K. BATES AND D. M. GRUEN, *J. Chem. Phys.* **70,** 4428–4429 (1979).
12. J. K. BATES AND D. M. GRUEN, *High Temp. Sci.* **10,** 27–43 (1978).
13. J. K. BATES AND D. M. GRUEN, *J. Mol. Spectrosc.* **78,** 284–297 (1979).
14. L. B. KNIGHT AND J. STEADMAN, *J. Chem. Phys.* **76,** 3378–3384 (1982).
15. D. W. GREEN, W. KORFMACHER, AND D. M. GRUEN, *J. Chem. Phys.* **58,** 404–405 (1973).
16. R. W. MARTIN AND A. J. MERER, *Canad. J. Phys.* **51,** 125–143 (1973).
17. R. W. MARTIN AND A. J. MERER, *Canad. J. Phys.* **51,** 634–643 (1973).
18. D. L. ALBRITTON, A. L. SCHMELTEKOPF, W. J. HARROP, R. N. ZARE, AND J. CZARNY, *J. Mol. Spectrosc.* **67,** 157–184 (1977).
19. L. VESETH, *Phys. Scr.* **12,** 125–128 (1975).
20. R. N. ZARE, A. L. SCHMELTEKOPF, W. J. HARROP, AND D. L. ALBRITTON, *J. Mol. Spectrosc.* **46,** 37–66 (1973).
21. A. S-C. CHEUNG, R. C. HANSEN, AND A. J. MERER, *J. Mol. Spectrosc.* **91,** 165–208 (1982).
22. A. S-C. CHEUNG, A. W. TAYLOR, AND A. J. MERER, *J. Mol. Spectrosc.* **92,** 391–409 (1982).
23. D. COSSART, H. LAVENDY, AND J. M. ROBBLE, *J. Mol. Spectrosc.* **99,** 369–406 (1983).
24. G. HERZBERG, "Spectra of Diatomic Molecules," 2nd ed., pp. 240–245, Van Nostrand, Princeton, New Jersey, 1950.
25. I. KOPP AND J. T. HOUGEN, *Canad. J. Phys.* **45,** 2581–2596 (1981).
26. J. H. VAN VLECK, *Rev. Mod. Phys.* **23,** 213–227 (1951).
27. R. S. MULLIKEN AND A. CHRISTY, *Phys. Rev.* **38,** 87–119 (1931).
28. A. BUDO AND I. KOVACS, *Phys. Z.* **45,** 122–126 (1944).
29. J. P. CHANDLER, "STEPT: A Family of Routines for Optimization and the Fitting of Data," Catalog #307, Quantum Chemistry Program Exchange, Department of Chemistry, Indiana University, Bloomington, Indiana, 1975.
30. D. W. MARQUARDT, *J. Soc. Indust. Appl. Math.* **11,** 431–441 (1963).
31. T. M. DUNN, *in* "Physical Chemistry—An Advanced Treatise" (H. Eyring, D. Henderson, and W. Jost, Eds.), Vol. V, pp. 205–286, Academic Press, New York, 1970.
32. T. M. DUNN, *in* "Proceedings, XIIIth Colloquium Spectrocopicum Internationale, P5821 Ottawa, 1967," pp. 363–369, Adam Hilger, London, 1967.
33. H. G. POWELL, *Proc. Phys. Soc.* **57,** 32–45 (1945).
34. C. K. JORGENSEN, "Modern Aspects of Ligand Field Theory," Part V, p. 513, American Elsevier, New York, 1971.
35. J. H. VAN VLECK, *Phys. Rev.* **33,** 467–506 (1929).
36. C. J. CHEETHAM AND R. F. BARROW, *Adv. High Temp. Chem.* **1,** 7–41 (1967).
37. R. C. CARLSON AND T. M. DUNN, submitted for publication.
38. A. ADAMS, W. KLEMPERER, AND T. M. DUNN, *Canad. J. Phys.* **46,** 2213–2220 (1968).
39. J. K. BATES, "Optical Emission Spectra of Diatomic Metal Nitrides," Ph.D. Dissertation, The University of Michigan, 1975.
40. D. N. DAVIS, *Astrophys. J.* **106,** 28–75 (1947).